Forest Ecology and Management 597 (2025) 123170

Contents lists available at ScienceDirect

Forest Ecology and Management

journal homepage: www.elsevier.com/locate/foreco

Nitrogen fertilization has a small but detectable effect on the spectral properties of needles in Norway spruce

Jussi Juola [a,*], Miina Rautiainen [a], Heli Peltola [b], Samuli Launiainen [c], Aarne Hovi [a]

[a] Department of Built Environment, School of Engineering, Aalto University, PO Box 14100, Aalto 00076, Finland
[b] School of Forest Sciences, University of Eastern Finland, PO Box 111, Joensuu 80101, Finland
[c] Bioeconomy and Environment, Natural Resources Institute Finland, Latokartanonkaari 9, Helsinki 00790, Finland

ARTICLE INFO

Keywords:
Hyperspectral
Spectroscopy
Reflectance
Albedo
Coniferous
Foliage
Nutrient

ABSTRACT

Optical remote sensing has been proposed as a tool to guide precise application of fertilizers; however, the effects of nitrogen (N) fertilization on the spectral properties of coniferous needles from mature forests are not known. In this extensive pilot study, we present how N fertilization affects the spectral properties, nutrient content, and morphological properties of Norway spruce needles collected from a controlled fertilization experiment in Finland. We found small mean differences (<3 % across the 400–2500 nm range) in reflectance, transmittance, and albedo spectra between the needles collected from fertilized and unfertilized plots. In addition, the results suggest a saturation in the spectral changes beyond moderate (<200 kg N ha^{-1}) levels of N fertilization. The needle spectra enabled predicting morphological properties using partial least squares regression. Specific leaf area and water content showed moderate-to-good generalization (R^2 values of 0.7 and 0.8, respectively) with low-to-very-low relative RMSEP-% values (6.2 % and 2.2 %, respectively) and narrow confidence intervals (4.8–7.4 % and 1.5–2.8 %, respectively). Nitrogen fertilization had a statistically significant effect on spectra only in current-year needles. We found that an absorption feature centered between 1112–1272 nm showed the best accuracy (83.3 %) in differentiating current-year needles collected from fertilized and unfertilized plots. Our results highlight that N fertilization has a small yet detectable effect on the spectral properties of needles in Norway spruce trees which could be used to develop remote sensing applications for assessing N fertilization in forests.

1. Introduction

Nitrogen (N) plays a crucial role in terrestrial carbon dynamics (Heimann and Reichstein, 2008), photosynthetic capacity (Reich et al., 1994), and net primary production (Field and Mooney, 1986). In boreal forests growing on mineral soils, it is also the main growth limiting nutrient (Tamm, 1991; Saarsalmi and Mälkönen, 2001). Therefore, N fertilization increases the growth of boreal forests growing on mineral soils and can contribute to climate change mitigation through enhanced carbon (C) sequestration and wood production (Hyvönen et al., 2008). However, too intensive fertilization may have adverse effects on the environment, such as increasing greenhouse gas emissions and nutrient export to water courses (Saarsalmi and Mälkönen, 2001; Hedwall et al., 2014; Håkansson et al., 2021; Huttunen et al., 2023). This calls for development of precision fertilization schemes, in which the fertilizer dose and type are scaled to the actual nutrient demand and nutrient supply of the forest stand, or even that of individual trees (Muhonen et al., 2025). This would also increase the cost-efficiency and resource-efficiency of fertilization (Boeraeve et al., 2025).

Optical remote sensing could be used as a tool to guide precise application of fertilizers, particularly in agriculture (Weiss et al., 2020) but also in forestry. The canopy level spectral reflectance properties respond both to changes in the canopy structure, leaf morphology and leaf nutrient content, which all may be affected by the nutrient status (Curran, 1989). Thus, the key to applying remote sensing in precision fertilization is to develop a quantitative understanding of how a specific fertilization treatment affects the spectral properties of individual trees and forest stands. Although leaf-level spectral properties do not directly scale to the canopy level (Knyazikhin et al., 2013), quantifying the response of leaf-level spectral properties to fertilization is a necessary building-block to develop such understanding. Previous studies have demonstrated that leaf-level spectroscopic measurements can generally

* Corresponding author.
E-mail address: jussi.juola@aalto.fi (J. Juola).

https://doi.org/10.1016/j.foreco.2025.123170
Received 6 June 2025; Received in revised form 8 September 2025; Accepted 9 September 2025
Available online 16 September 2025

be used to estimate N content, specific leaf area, chlorophyll content, and other key traits of coniferous needles (Homolová et al., 2013; Lhotáková et al., 2021; Lukeš et al., 2013; Malenovský et al., 2013; Schlerf et al., 2010). Fertilization has been shown to significantly impact the needle morphology of, e.g., small Scots pine seedlings (Jokela et al., 1995) and young Sitka spruce trees (Chandler and Dale, 1995). However, its effect on the spectral properties of coniferous needles remains largely unknown due to lack of such studies.

In the pioneering study with small Engelmann spruce seedlings, Moran et al. (2000) reported a statistically significant spectral response to N fertilization near the red edge region. Yet, how needle spectra respond to N fertilization in mature coniferous forests has not been previously reported. Such information would provide the physical understanding of possibilities offered by remote sensing measurements to support precision fertilization. It could also improve the understanding of the effects of fertilization treatments on forest albedo, which is one of the important factors influencing the climate effects of forests and forest management (Bonan, 2008).

The primary goal of our study was to examine the effects of N fertilization on the spectral properties of needles of Norway spruce (*Picea abies* (L.) Karst.). It is widely distributed across Europe and has crucial economic and ecological value. In this study, we measured the spectral properties, nutrient contents, and morphological properties of needles sampled from a controlled fertilization experiment in eastern Finland. More specifically, our research questions were: 1) How does N fertilization and the nutrient status affect the spectral characteristics of Norway spruce needles in the visible to shortwave-infrared region (400–2500 nm)?, 2) To what extent can N fertilization treatment be differentiated from the spectral properties?, and 3) Which wavelengths or regions of the spectrum are influential for retrieving leaf biochemical and morphological traits? Our study contributes to understanding the physical mechanisms underlying the differences in the spectral reflectance and albedo of fertilized and unfertilized boreal Norway spruce stands. To our knowledge, this is the first study to report the effects of varying N fertilization levels on the needle spectra of Norway spruces in a controlled experimental setting.

2. Materials and methods

2.1. Study area and measurements

2.1.1. Fertilization experiment

The fertilization experiment (10 ha in size) used in this study was established in summer 2019 in a mature boreal Norway spruce dominated forest (Muhonen et al., 2025). It is located on mineral soil, on a mesic site fertility type (Myrtillus-type; site type classification of Cajander 1949) in Savonranta, Eastern Finland (62,139028 N, 29, 149086 E, altitude 120–140 m a.s.l.) (Fig. 1). Mean stem diameter was 21 cm and stand density 455 trees ha^{-1}. Each fertilization treatment, with target fertilizer doses of 0, 150, and 200 kg N ha^{-1}, included three replicate blocks (each one hectare in size) and three circular plots (7.98 m radius, area of 200 m^2) per block. Tree attributes were measured before fertilization and subsequently on an annual basis. The fertilization in 2019 was done using helicopter spreading, using a commercially available fertilizer, YaraMila Metsän NP, which includes N 25 % (Nitrate nitrogen 12 %, Ammonium nitrogen 13 %), phosphorus (P) 2 %, magnesium (Mg) 1 %, boron (B) 0.3 % and zinc (Zn) 0.1 % (for details see Muhonen et al., 2025). The spatial evenness of the helicopter-spread fertilizer dose was measured with textile funnels immediately after fertilization. The actualized fertilizer levels, ranging between 0–426 kg N ha^{-1}, were used in our analyses. Based on the actualized levels, we selected 18 circular plots that maximized the variation in the fertilizer level and provided equal number of plots (n = 6) with 0 kg N ha^{-1}, $0 < x \leq 200$ kg N ha^{-1}, and > 200 kg N ha^{-1} (Fig. 1). The mean plant area index for the 18 circular plots was 3.8 m^2 m^{-2} (range 2.6–5.3). Each circular plot had two dominant trees that were sampled for needles (i.e., sample tree, see Section 2.1.2 for details). All measurements in this study were conducted between 15.–26.7.2024.

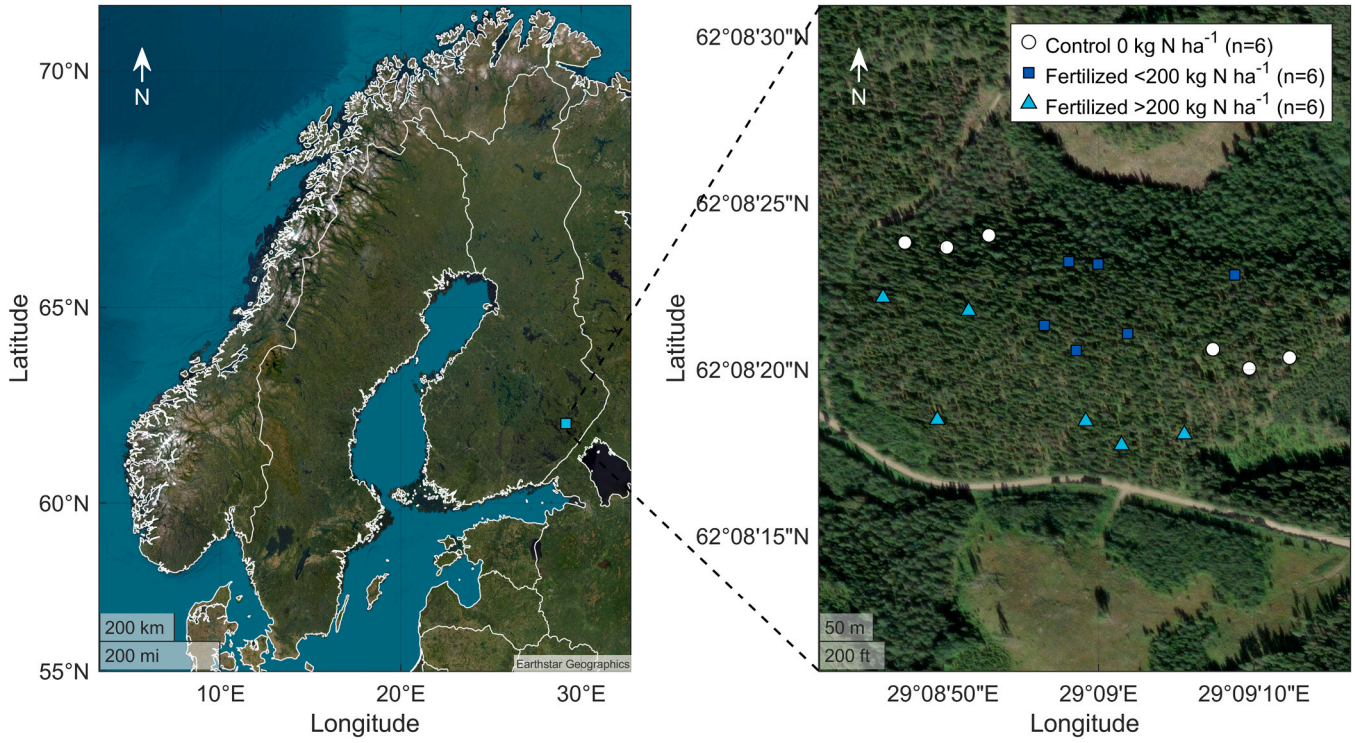

Fig. 1. Left: Location of the study site in eastern Finland (cyan square). Right: High spatial resolution image of the 18 circular plots used for sampling. White circles (n = 6) indicate unfertilized control plots (0 kg N ha^{-1}), while blue squares (n = 6) and cyan triangles (n = 6) represent fertilized plots with < 200 kg N ha^{-1} and > 200 kg N ha^{-1}, respectively. Images were produced using MATLAB's satellite basemap, hosted by Esri.

2.1.2. Needle samples for spectral, morphological, and nutrient analyses

Samples of top-of-canopy (sun-exposed) needles were collected using a branch cutter extendable up to 20 m. South-facing branches were cut from the upper third of the crown of each sample tree. Samples included two needle age cohorts: current-year (c0) and previous-year (c1) needles, used for spectral, morphological, and nutrient content measurements. Since two dominant Norway spruce trees were sampled per plot, this yielded 72 samples in total (18 plots × 2 dominant trees × 2 needle age cohorts).

To obtain sufficient number of needles for all measurements, multiple branches per tree (3–5, depending on branch size and condition) were collected. The cut ends of the detached branches were immediately placed in water-filled tubes and stored inside cool boxes for short transport to laboratory facilities in Savonlinna, Finland. Upon arrival, branch bases were recut underwater to enhance water uptake and stored at 2°C in a dark cold room. Spectral and morphological measurements, as well as preparation of samples for the nutrient analyses, were all done during the same day, so that the maximum duration of cold storage was 11 h. Shoots were removed from cold storage just before measurements to minimize physiological changes, such as water loss.

For the spectral measurements (Section 2.1.3), one branch per tree was selected, and one shoot per needle age cohort (consecutive shoots) was randomly chosen. The morphological measurements (Section 2.1.4) used three additional shoots per age cohort from the same branch. These four shoots per age cohort were pooled, and one was randomly selected for the spectral measurements, with the remaining three used for the morphological measurements. The nutrient analysis (Section 2.1.4) required at least 0.5 liter of unpressed shoots per age cohort from the remaining branches per tree. For the previous-year samples, occasional Lammas growth (late summer shoots) was possibly included in the samples for nutrient measurements as they were very difficult to distinguish. Only visibly healthy foliage samples were measured.

2.1.3. Spectral measurements of needles

We measured reflectance (directional-hemispherical reflectance factor, DHRF) and transmittance (directional-hemispherical transmittance factor, DHTF) spectra (350–2500 nm) of the needles (Schaepman-Strub et al., 2006). Needle albedo, representing average scattering behavior, was calculated as the sum of reflectance and transmittance.

Measurements were performed using an ASD RTS-3ZC integrating sphere (serial no. 12152804) attached to an ASD FieldSpec4 spectroradiometer (serial no. 18641), which was allowed to warm up for at least one hour. The needle sample was illuminated with a direct beam from a 10 W collimated ASD CL-10 halogen light source. The beam diameter on the sample was approximately 7 mm in the reflectance and transmittance measurements (Hovi et al., 2018). The spectral resolution of the instrument was 3 nm (≤1000 nm) and 10 nm (>1000 nm), and the sampling interval was 1.4 nm (≤1000 nm) and 2 nm (>1000 nm), with output data interpolated at 1 nm intervals. Representative and healthy needles from the central part of the shoots were carefully detached using tweezers to avoid altering spectral properties, then mixed randomly before measurement. The needles were arranged evenly in 0.3 mm thick sample holders (needle carriers) with a spacing of approximately 0.5–1 needle width (i.e., gap fraction approximately 0.33–0.5) (Yanez-Rausell et al., 2014). Metal spacers (0.6 mm) between carrier plates prevented physical compression and ensured consistent spacing between measured samples. A visual representation of the needle carriers for ASD RTS-3ZC integrating sphere is available in Fig. 1 in Hovi et al. (2020).

Reflectance and transmittance were measured on both sides of the sample, with white reference measurements taken for both reflectance and transmittance using a calibrated 1.25-inch Spectralon® diffuse reflectance standard (serial no. 99AA02–1115–3079, 99 % nominal reflectance). Stray light in the reflectance measurements, caused by imperfect collimation of the light source, was determined with a photon trap attached to the integrating sphere. The measurement protocol for the spectral measurements in this study is the same as applied in Hovi et al. (2020) and Hovi et al. (2022a). The spectrometer's raw readings were processed into reflectance (R) and transmittance (T) using the following standard processing formulas that take into account the influence of gaps in the needle sample on the measured signal:

$$R = \frac{S_R}{S_{ref\_R}} \frac{1}{1 - P_{gap\_R}} R_{ref} \quad \text{, and} \tag{1}$$

$$T = \left(\frac{S_T}{S_{ref\_T}} - P_{gap\_T} \right) \frac{1}{1 - P_{gap\_T}} R_{ref}, \tag{2}$$

where S_R and S_T are the raw readings (in digital numbers) from reflectance and transmittance measurements, S_{ref_R} and S_{ref_T} correspond to the white reference readings, R_{ref} is the reflectance of the calibrated white reference panel, and P_{gap_R} and P_{gap_T} are the sample's gap fractions. Stray light was subtracted from S_R and S_{ref_R} before calculations. The reflectance and transmittance of the two sides of the sample were averaged to obtain one reflectance spectrum and one transmittance spectrum per sample, respectively.

The gap fractions (P_{gap_R} and P_{gap_T}) were determined by scanning the needle carriers with a digital film scanner (Epson Perfection V550, 800 dpi) and applying a gray-level threshold of 229 (Hovi et al., 2022b) to binarize the scanned images. A photogrammetrically calibrated camera, needle carrier, and the integrating sphere were used to measure the relative irradiance distribution of the illumination beam within the carrier's coordinate system (Hovi et al., 2020). The irradiance distribution was then mapped onto the binary image to calculate the gap fraction of a needle sample within the area illuminated by the light source. In this study, the average gap fractions for reflectance and transmittance were 0.36 and 0.35, respectively, typically corresponding to seven needles placed onto the carrier. Finally, to correct for a small inherent bias in transmittance measurements performed with the ASD RTS-3ZC integrating sphere (Hovi et al., 2020), we also applied an empirical correction that reduced the transmittance spectra at all wavelengths by 5.5 % in relative terms, ensuring non-negative absorption (i.e., albedo less than 1) in all wavelengths.

2.1.4. Nutrient and morphological measurements of needles

The current-year (c0) and previous-year (c1) needle samples used for nutrient analyses were oven-dried (50°C) for 72 h and grinded, and nutrient (C, N, P, K, B, Al, Ca, Cu, Fe, Mg, Mn, S, and Zn) analyses were done at the laboratory of the University of Eastern Finland. The C and N contents were measured using a Elementar vario MICRO cube and the rest with Thermo Scientific iCAP 7200 ICP-OES.

For morphological measurements, the needles were randomly picked from the three shoots of each sample tree and divided into two subsets: five and 50 needles. The first subset was used to determine the projected-to-total needle area conversion factor, as such a number of needles has been shown to provide a reliable estimate of total needle area (e.g., Homolová et al., 2013).

The major and minor diameters of the needles were manually measured with a digital caliper before scanning with a digital film scanner (Epson Perfection V550, 800 dpi). The scanned images were processed using an in-house MATLAB image analysis procedure to determine the projected area and length of each needle in the sample. The total needle area (NA_T) was calculated using the formula proposed by Sellin (2000), assuming a needle cross-section approximated as a parallelepiped:

$$NA_T = 2L\sqrt{D_1^2 + D_2^2}, \quad (3)$$

where L is the length and D_1 and D_2 are the major and minor diameters of the needle, respectively.

The second subset of 50 needles was used to determine the projected area-to-dry mass ratio. The 50 needles were first weighed for fresh mass using a laboratory precision scale (Radwag PS 1000.R2, readability interval d = 0.001 g). The needles were then scanned (Epson Perfection V550, 800 dpi) before being dried in a laboratory oven (60°C) for 48 h. After drying, the needles were reweighed for dry mass. Specific leaf area (SLA) and water content (WC) were calculated as:

$$SLA = \frac{C_5 \times NA_{P\_50}}{m_{dry}}, \text{and} \quad (4)$$

$$WC = \frac{m_{fresh} - m_{dry}}{m_{fresh}} \times 100\%, \quad (5)$$

where C_5 is the projected to total area conversion factor estimated using the subset of five needles, NA_{P_50} is the projected area calculated using

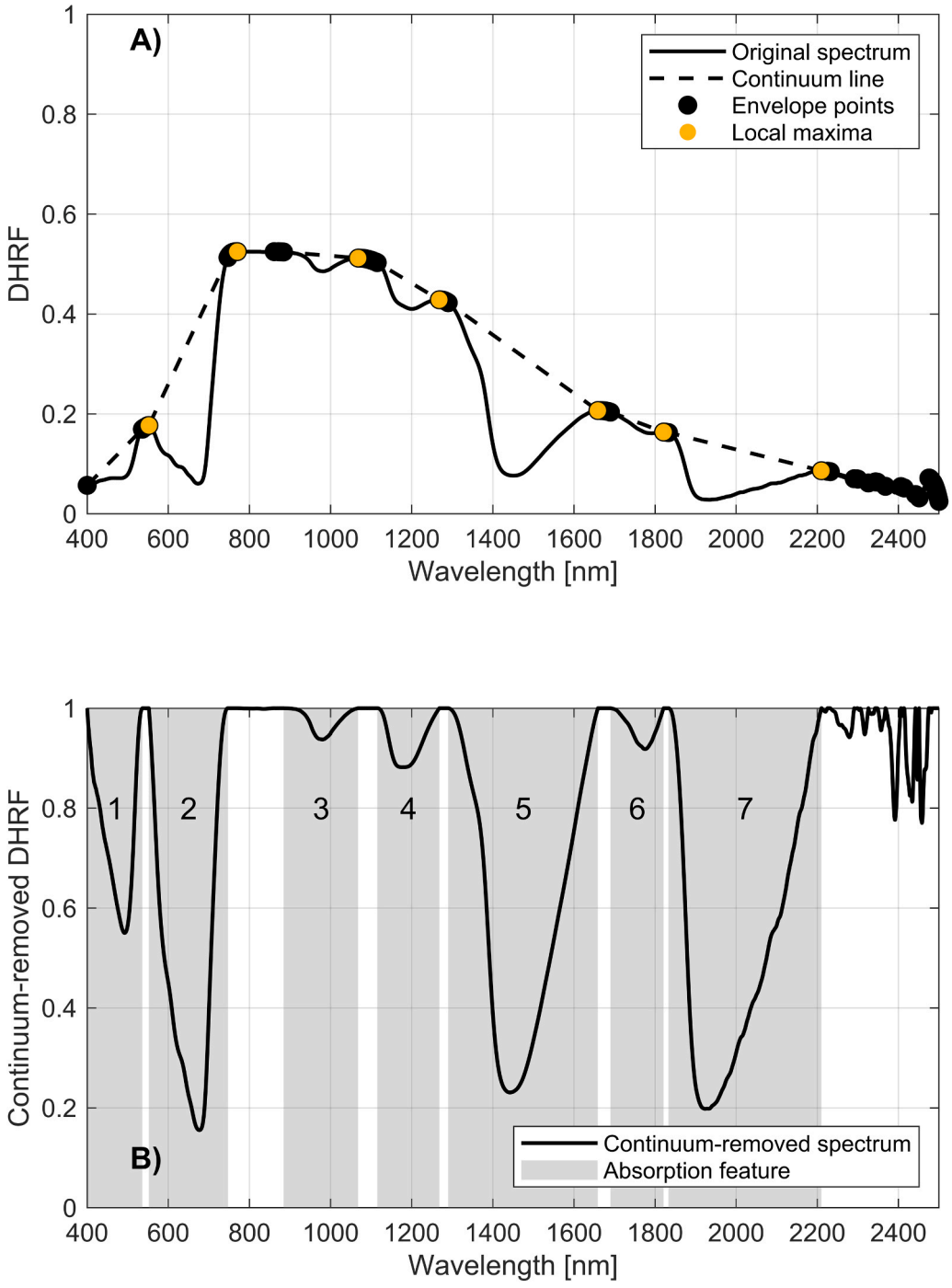

Fig. 2. Visual example of the continuum removal showing: A) the original reflectance (directional-hemispherical reflectance factor, DHRF) spectrum (solid line) and the continuum line (dashed line) linearly interpolated using the local maxima (yellow points) and supportive envelope points (black points), and B) the continuum-removed DHRF spectrum (solid line) and seven individual absorption features (numbered solid gray regions) within the 400–2500 nm range. The absorption features were calculated between the two closest local maxima or envelope endpoints seen in A.

the subset of 50 needles, and m_{dry} and m_{fresh} are the dry and fresh mass of the 50 needles, respectively.

2.2. Data analyses

2.2.1. Overview of analyses

We conducted a series of analyses to study how N fertilization, morphological properties, and nutrient content influence the spectral characteristics of Norway spruce needles. First, we reduced noise and extracted absorption features by filtering the spectral data and applying continuum removal, respectively (Section 2.2.2). Next, we analyzed the effects of N fertilization on spectra, nutrient content, and morphological properties by categorizing needle samples into three fertilization levels (0 kg N ha^{-1}, 0 < x ≤ 200 kg N ha^{-1}, and >200 kg N ha^{-1}) based on the fertilizer doses applied at each plot and by identifying statistically significant differences between samples collected from fertilized and unfertilized plots (Section 2.2.3). Then, we assessed the separability of needles samples collected from fertilized and unfertilized plots based on their spectral properties by employing a binary classifier (Section 2.2.4). Finally, we estimated needle nutrient content and morphological properties and identified key wavelengths or wavelength regions for retrieving biophysical and biochemical traits by applying partial least squares regression to the spectral data (Section 2.2.5). All analyses were carried out using MATLAB (Version: 24.2.0.2740171 (R2024b) Update 1).

2.2.2. Preprocessing of spectral data

The reflectance and transmittance spectra of needles were first filtered with the Savitzky-Golay filter (Savitzky and Golay, 1964), with 2nd order polynomial and window size of 15 nm for 350–1000 nm and 39 nm for 1000–2500 nm. We excluded wavelengths below 400 nm due to poor signal-to-noise ratio.

Next, the reflectance, transmittance, and albedo spectra were continuum-removed (Clark and Roush, 1984) to extract and analyze absorption features in the 400–2500 nm range. We applied continuum removal by dynamically identifying seven local maxima that lie between known major foliage absorption features: 1) 500–600 nm, 2) 700–900 nm, 3) 1000–1200 nm, 4) 1200–1400 nm, 5) 1600–1750 nm, 6) 1800–1900 nm, and 7) 2150–2250 nm (Fig. 2A). We used linear interpolation, with an envelope operation before and after each maximum to account for the spectral curvature. The envelope operation ensured that when the observed spectrum was divided by the continuum line, the normalized spectrum remained between 0 and 1, preventing the continuum from cutting below the original spectrum (Fig. 2). The dynamic identification of local maxima accounted for variations in sample properties (e.g., nutrient and water content) that influence absorption widths and positions. We calculated eight Area Under the Curve (AUC) features from the continuum-removed spectra via trapezoidal method: one for the entire continuum-removed spectrum (between 400 nm and the seventh local maximum) and seven corresponding to the individual absorption features (Fig. 2B). The seven individual absorption features were always calculated between the two closest left and right endpoints within the feature wavelength range (Fig. 2A). The wavelength ranges of the left and right continuum endpoints for the seven absorption regions in the reflectance, transmittance, and albedo spectra are presented in Table A.1 in Appendix A. Based on the continuum end points (Table A.1), wavelengths between 400 and 2234 nm were used in the following classification (Section 2.2.4) and regression (Section 2.2.5) analyses to minimize the negative influence of noise in the low and high ends of the spectrum.

2.2.3. Statistical analyses

The reflectance, transmittance, and albedo spectra of samples collected from the highly (>200 kg N ha^{-1}) and moderately (0 < x ≤ 200 kg N ha^{-1}) fertilized plots were compared to the needle samples collected from unfertilized (control) plots (0 kg N ha^{-1}) using a two-sided Mann-Whitney U test (0 kg N ha^{-1} vs. 0 < x ≤ 200 kg N ha^{-1}, and 0 kg N ha^{-1} vs. >200 kg N ha^{-1}). The same test was applied to the 13 nutrients, morphological properties (SLA and WC), and eight AUC features from the continuum removal analysis. A nonparametric test was chosen due to violations of normality assumptions across the tested traits.

2.2.4. Classification of needle samples from fertilized and unfertilized plots

To demonstrate the potential of spectral data in distinguishing needle samples from fertilized and unfertilized plots, we report the results of the highest-performing binary classifier identified: the support vector machine (SVM). For a detailed explanation of SVM in various case studies, see Brereton and Lloyd (2010). We used a SVM with a linear kernel function, a uniform prior distribution, an automatic scale factor using a heuristic procedure, and standardized features (by removing the mean and scaling to unit variance). We used wavelengths between 400 and 2234 nm to identify the best features and to minimize the negative influence of noise that typically occurs in the high and low ends of the spectrum (based on Section 2.2.2). Model performance was assessed using leave-one-out cross-validation (LOOCV), with classification accuracy evaluated through balanced accuracy (BA), user's accuracy (UA), producer's accuracy (PA), and F1-score. The UA measures the proportion of correctly predicted positives out of all predicted positives, while the PA reflects the proportion of correctly predicted positives out of all actual positives. The F1-score is the harmonic mean of UA and PA. All four metrics are calculated from the true positives (TP), true negatives (TN), false positives (FP), and false negatives (FN) as follows:

$$BA = \frac{\frac{TP}{TP+FN} + \frac{TN}{TN+FP}}{2}, \tag{6}$$

$$UA = \frac{TP}{TP+FP}, \tag{7}$$

$$PA = \frac{TP}{TP+FN}, \tag{8}$$

$$F1 = 2 \times \frac{UA \times PA}{UA+PA}. \tag{9}$$

2.2.5. Estimation of morphological properties and nutrient contents from spectral data

We used partial least-squares regression (PLSR) to estimate morphological properties and nutrient contents of needles from our reflectance and albedo spectra (n = 72). Again, we used wavelengths between 400 and 2234 nm to minimize the negative influence of noise in the spectra. Transmittance spectra were excluded because transmittance is already accounted for in albedo.

In addition to estimating morphological properties and needle nutrient content, we used PLSR to identify key wavelengths for each estimated trait using average Variable Importance in Projection (VIP) scores (Eriksson et al., 2013; Wold et al., 1993). PLSR-generated weights were used to calculate the VIP scores, which directly link the features or spectral wavelengths to the needle constituents (Haaland and Thomas, 1988). Wavelengths with VIP scores above 1 were considered important for the model (Chong and Jun, 2005; Eriksson et al., 2013; Gosselin et al., 2010).

We evaluated model performance using the point estimate of prediction error and its mean squared error (MSE) estimate, both derived from the novel nested cross-validation scheme by Bates et al. (2024) (see Algorithm 1 in their Supplementary Appendix). Their nested cross-validation provides accurate confidence intervals for the point estimate of prediction error and is particularly effective for small datasets, where overfitting is a concern. In the outer loop, the nested scheme randomly splits data into k outer folds, holding out one fold as a test set while using the remaining $k-1$ folds for training. This process is repeated r times. The inner loop then fits the model on the $k-1$ outer folds using another k'-fold cross-validation loop, repeated r' times, ensuring that the holdout fold from the outer loop is never used in the inner loop. The inner cross-validation step was used to determine the optimal number of PLSR components by minimizing the residual sum of squares trained on the $k'-1$ folds, averaged over r' repetitions. To further prevent overfitting, we applied the one standard error rule, selecting the smallest number of components within one standard error of the optimal value (Hastie et al., 2009). This nested cross-validation scheme ensured that component selection was performed independently for each outer fold.

Using squared error loss, the point estimate corresponded to the mean squared prediction error (MSPE) from the repeated inner cross-validation step. Both MSPE and its MSE estimate were used to compute 95 % confidence intervals for the point estimate of prediction error, following Eq. 9 in Bates et al. (2024). Additionally, we calculated the root mean square error of prediction (RMSEP) in the original measurement units, the relative RMSEP (RMSEP-%) as a percentage of the data range, and the coefficient of determination (R^2, based on sum of squares) for the mean fitted point estimate vs. observed values.

We used 10-fold cross-validation (k and k') for both the outer and inner loops, with $r = 200$ outer loop repetitions and $r' = 50$ inner loop repetitions. The maximum number of components considered for the PLSR model in the inner loop of the nested cross-validation scheme was 20 (Burnett et al., 2021). To remove bias from the prediction error, we performed 10-fold cross-validation, averaging the results over 100 repetitions (Bates et al., 2024).

3. Results

3.1. Effect of fertilization on spectral and morphological properties and nutrient contents of needles

3.1.1. Reflectance, transmittance, and albedo spectra of needles

We found small mean differences (<3 % across the 400–2500 nm range) in reflectance, transmittance, and albedo spectra between Norway spruce needles collected from fertilized and unfertilized plots (Fig. 3, Fig. 4). Even smaller spectral differences (<1 % across the 400–2500 nm range) were observed between samples collected from the

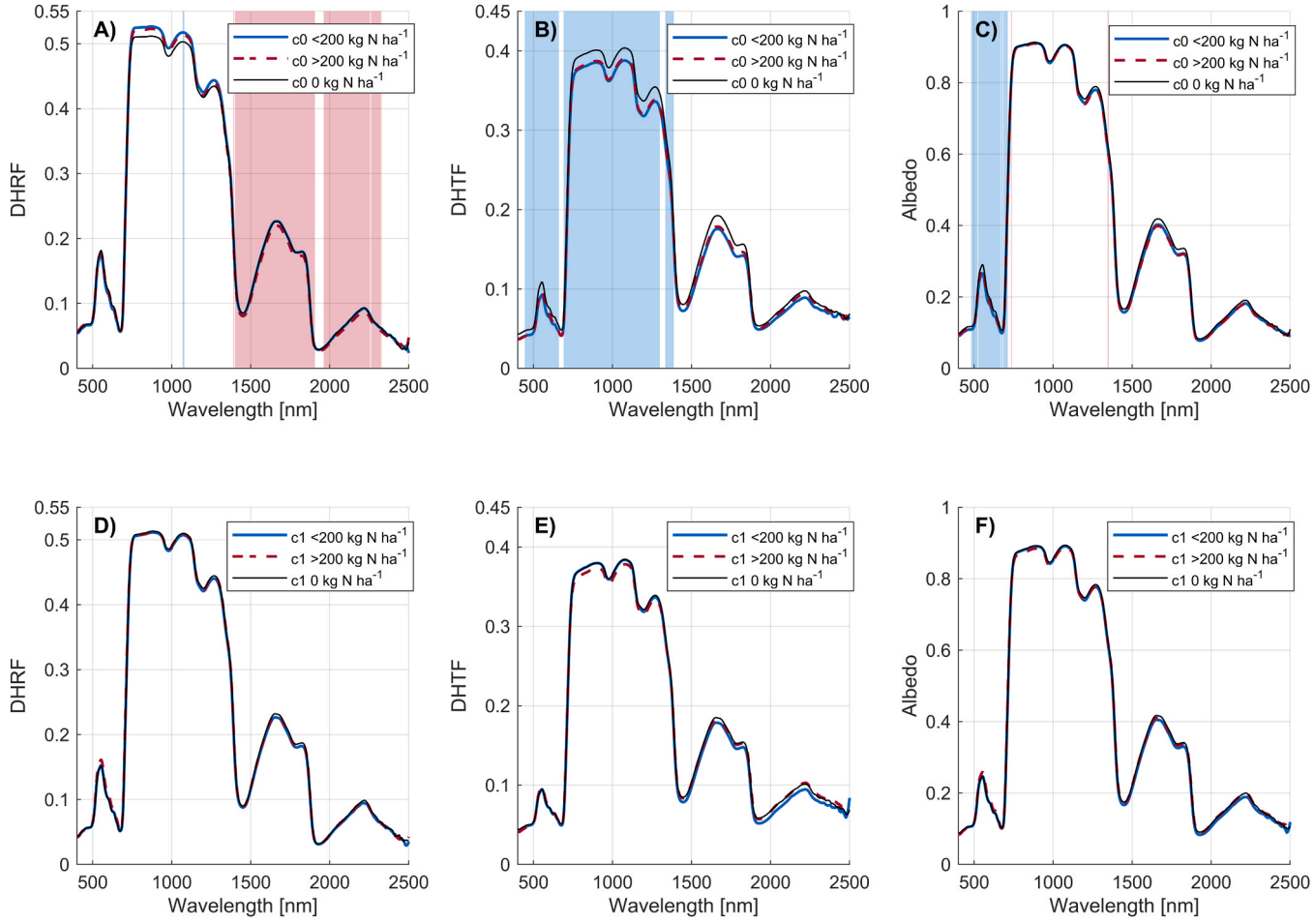

Fig. 3. Mean reflectance (directional-hemispherical reflectance factor, DHRF), transmittance (directional-hemispherical transmittance factor, DHTF), and albedo spectra of needle samples collected from unfertilized and fertilized plots. A–C show results for current-year (c0) needles, and D–F show results for previous-year (c1) needles. The solid black line represents the mean spectrum of needle samples from unfertilized (0 kg N ha^{-1}) plots, the solid blue line represents samples from fertilized plots with < 200 kg N ha^{-1} , and the dashed red line represents samples from fertilized plots with > 200 kg N ha^{-1} . Shaded blue and red areas indicate wavelengths for samples from fertilized plots with < 200 kg N ha^{-1} and > 200 kg N ha^{-1} , respectively, which differ significantly from samples from unfertilized (0 kg N ha^{-1}) plots (Mann-Whitney U test, at $p < 0.05$ significance level).

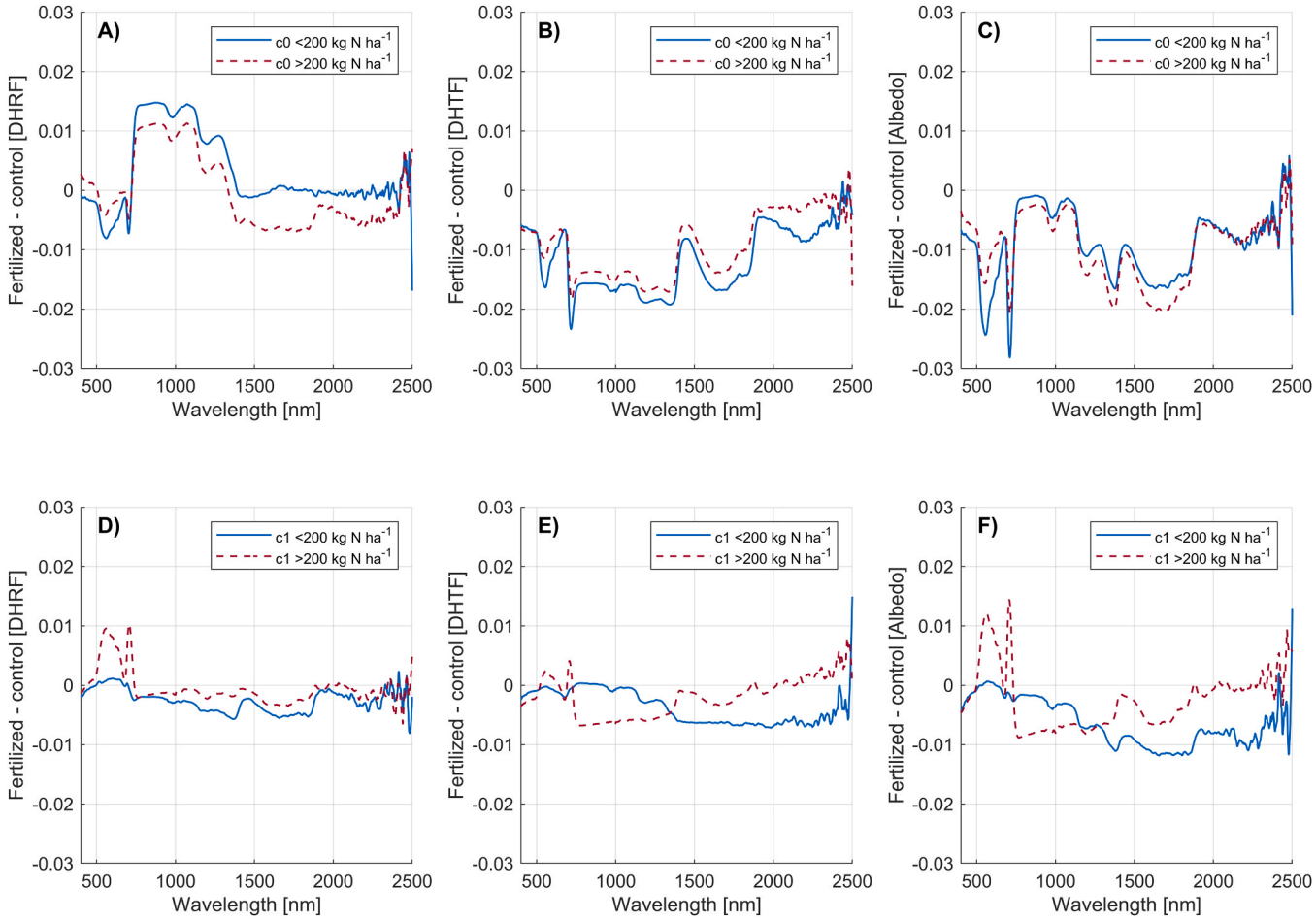

Fig. 4. Mean difference in reflectance (directional-hemispherical reflectance factor, DHRF), transmittance (directional-hemispherical transmittance factor, DHTF), and albedo spectra between needles collected from fertilized and unfertilized plots. A–C show results for current-year (c0) needles, while D–F show results for previous-year (c1) needles. The solid blue line is the mean difference for the needle samples collected from < 200 kg N ha^{-1} and 0 kg N ha^{-1} plots, and the dashed red line is the mean difference for the needle samples collected from > 200 kg N ha^{-1} and 0 kg N ha^{-1} plots.

Table 1
Statistical comparison (Mann-Whitney *U* test, at $p < 0.05$ significance level) of AUC values of samples collected from plots with moderate and high fertilization intensity (<200 kg N ha^{-1} and >200 kg N ha^{-1}) against the AUC values of samples collected from unfertilized plots (0 kg N ha^{-1}). The AUC values were calculated from continuum-removed reflectance (DHRF), transmittance (DHTF), and albedo spectra across seven absorption features between 400–2500 nm. Statistically significant differences ($p < 0.05$) are marked with an asterisk.

	AUC [DHRF]				AUC [DHTF]				AUC [Albedo]			
	p-value				p-value				p-value			
	Current-year (c0)		Previous-year (c1)		Current-year (c0)		Previous-year (c1)		Current-year (c0)		Previous-year (c1)	
Absorption feature	**< 200**	**> 200**	**< 200**	**> 200**	**< 200**	**> 200**	**< 200**	**> 200**	**< 200**	**> 200**	**< 200**	**> 200**
1	0.44	0.47	0.84	0.54	0.08	0.47	0.89	0.44	0.21	0.67	0.89	0.51
2	**0.01***	0.14	0.71	0.51	0.05	0.14	0.54	0.67	0.21	0.8	0.8	0.16
3	**0.03***	**0.01***	0.51	0.75	0.14	0.07	0.37	0.8	**0.04***	**0.01***	0.47	0.93
4	**0.01***	**0.01***	0.37	0.54	0.06	**0.02***	0.21	0.62	**0.02***	**0.02***	0.31	0.44
5	**0.02***	**0.02***	0.75	0.84	0.07	0.1	0.26	0.54	0.26	0.8	0.84	0.16
6	0.8	0.47	0.71	0.71	0.29	0.14	0.29	0.8	0.47	0.98	0.89	0.58
7	0.84	0.17	0.19	0.26	**0.04***	0.26	0.84	0.98	0.19	0.21	0.4	0.54
1–7	0.07	0.24	0.29	0.44	**0.04***	0.16	0.54	0.89	0.98	0.8	0.58	0.4

plots with moderate and high fertilization intensity (i.e., <200 kg N ha^{-1} vs. >200 kg N ha^{-1}, respectively) (Fig. 3, Fig. 4). Wavelengths with statistically significant differences in reflectance were found in the shortwave-infrared (SWIR, 1100–2500 nm) region for current-year needles collected from plots with high fertilization intensity (Fig. 3A). In transmittance and albedo, wavelengths with statistically significant differences were primarily detected in the near-infrared (NIR, 700–1100 nm) and visible (VIS, 400–700 nm) regions, respectively, for current-year needles collected from plots with moderate fertilization intensity (Fig. 3B–C). In previous-year needles, statistically significant differences were not found for any of the spectral quantities (Fig. 3D–F).

For current-year needles, samples collected from fertilized plots exhibited up to ~1.5 % higher mean reflectance than the samples collected from unfertilized plots in the NIR and early SWIR regions (Fig. 4A). In terms of transmittance, current-year needle samples collected from fertilized plots showed up to ~2 % lower mean transmittance than the samples collected from unfertilized plots across the VIS–SWIR regions (Fig. 4B). A similar but even weaker difference was observed for previous-year needles (Fig. 4E). Overall, the albedo of current-year needle samples collected from fertilized plots was lower than that of the samples collected from unfertilized plots from the VIS to SWIR regions (Fig. 4C).

3.1.2. *Continuum-removed absorption features of needles*

Spectral feature analysis with continuum removal revealed statistically significant differences in the seven isolated absorption features between needle samples collected from fertilized and unfertilized plots, but only for current-year needles (Table 1). The most pronounced difference across all three spectral quantities (reflectance, transmittance, and albedo) was observed in the absorption feature four (Table 1), which spans approximately 1112–1272 nm at the beginning of the SWIR region (Table A.1 in Appendix A). Of the three spectral quantities, reflectance exhibited the strongest statistically significant difference when the two needle sample groups collected from fertilized plots

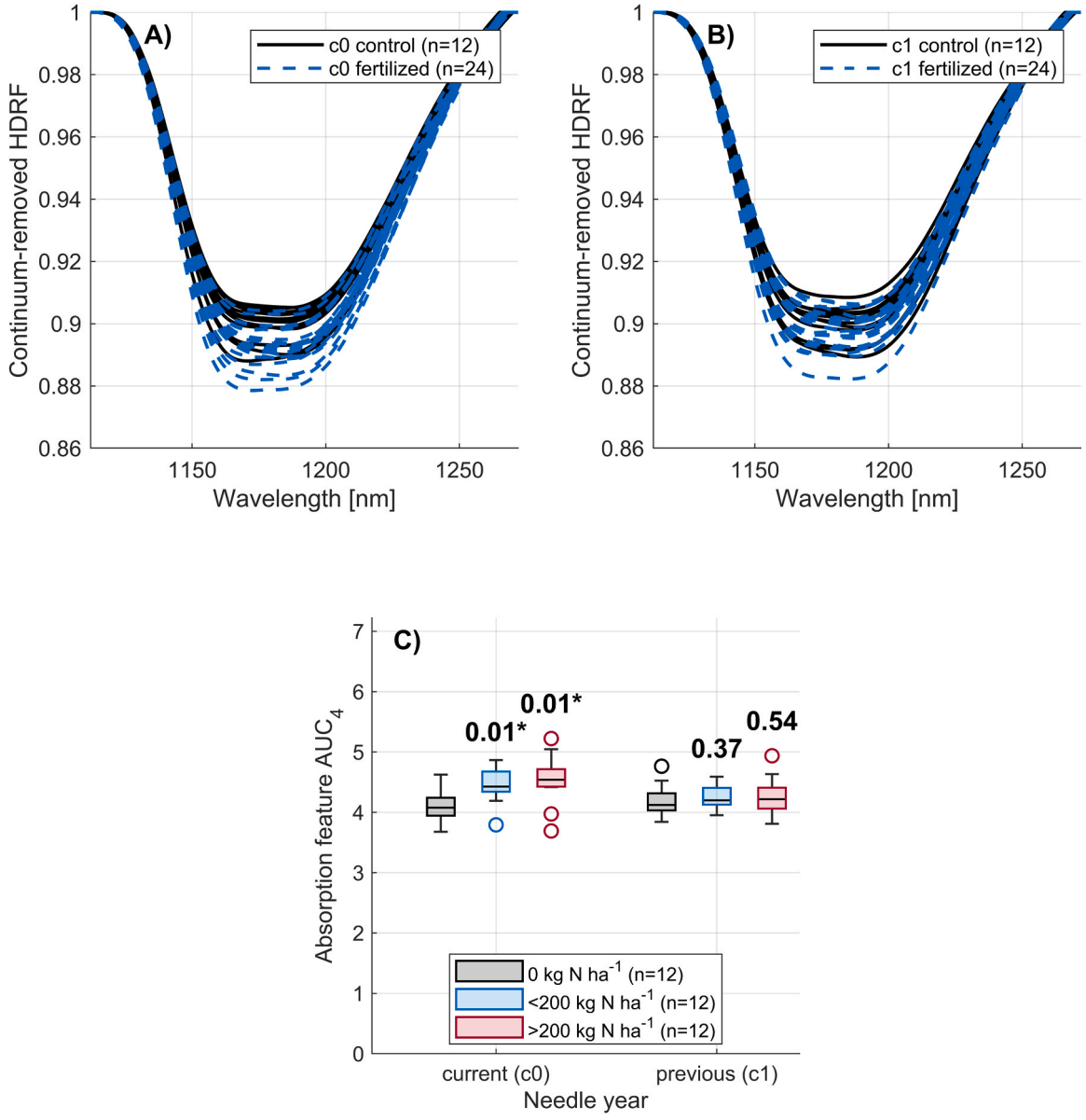

Fig. 5. Continuum-removed reflectance (directional-hemispherical reflectance factor, DHRF) spectra in the wavelength range of 1112–1272 nm for A) current-year and B) previous-year needle samples collected from fertilized (dashed blue lines) and unfertilized (solid black lines) plots. C) The corresponding area under the curve (AUC) value distributions are further divided into moderate (<200 kg N ha^{-1}) and high (>200 kg N ha^{-1}) fertilization intensity groups. The values in subfigure C) indicate p-values in the Mann-Whitney *U* test. Statistically significant differences ($p < 0.05$) are marked with an asterisk.

Table 2
Median values (with ranges) of measured morphological properties and nutrient contents for current-year (c0) and previous-year (c1) needle samples collected from fertilized and unfertilized (control) plots.

	Needle group			
	Current-year (c0)		Previous-year (c1)	
	Fertilized (n = 24)	Control (n = 12)	Fertilized (n = 24)	Control (n = 12)
Needle property	**Median (min–max)**	**Median (min–max)**	**Median (min–max)**	**Median (min–max)**
Specific Leaf Area, SLA [cm^2 g^{-1}]	90.1 (76.5–106.9)	95.8 (82.7–108.9)	83.2 (67.4–99.3)	87.8 (70.9–100.2)
Water Content, WC [%]	58.2 (53.2–60.8)	57.7 (54.5–62.4)	54.0 (49.8–57.3)	54.8 (50.8–58.8)
Nitrogen content, N [%]	0.91 (0.63–1.10)	0.90 (0.58–1.19)	0.82 (0.64–0.98)	0.76 (0.59–1.00)
Carbon content, C [%]	49.7 (48.6–50.5)	49.4 (48.9–49.9)	50.0 (48.9–50.7)	50.1 (48.8–50.8)
Potassium content, K [mg g^{-1}]	4.75 (3.14–7.30)	4.86 (3.74–7.23)	3.46 (2.09–5.39)	4.21 (2.55–6.13)
Phosphorus content, P [mg g^{-1}]	1.52 (1.06–1.97)	1.62 (1.04–1.90)	1.21 (0.86–1.57)	1.41 (0.95–1.71)
Aluminum content, Al [μg g^{-1}]	22.9 (12.5–38.3)	24.2 (16.7–72.9)	50.2 (28.3–127.5)	50.5 (22.5–107.7)
Boron content, B [μg g^{-1}]	10.1 (6.8–14.7)	4.8 (2.8–6.8)	19.6 (9.3–35.6)	4.2 (3.4–7.5)
Calcium content, Ca [μg g^{-1}]	2140.3 (1156.0–3403.3)	2627.5 (1315.2–10329.9)	5456.6 (3392.3–8143.0)	6092.9 (2437.8–11871.4)
Copper content, Cu [μg g^{-1}]	2.65 (1.30–4.80)	2.15 (1.40–2.90)	2.00 (1.00–6.70)	2.20 (1.30–24.30)
Iron content, Fe [μg g^{-1}]	17.9 (13.8–24.1)	19.8 (15.4–22.8)	24.3 (18.0–28.9)	23.9 (14.5–32.6)
Magnesium content, Mg [μg g^{-1}]	909.7 (571.0–1354.7)	968.0 (738.5–1297.1)	857.0 (448.9–1528.1)	1006.7 (715.6–1438.3)
Manganese content, Mn [μg g^{-1}]	336.4 (130.7–722.2)	559.2 (319.9–1577.2)	730.5 (316.7–2352.1)	1063.4 (495.0–2222.1)
Sulphur content, S [μg g^{-1}]	665.7 (490.0–830.8)	650.6 (522.4–824.0)	727.3 (566.2–865.3)	725.1 (586.6–817.2)
Zinc content, Zn [μg g^{-1}]	23.6 (10.7–35.9)	30.4 (20.6–37.4)	14.7 (5.8–33.4)	30.2 (11.0–38.4)

(<200 kg N ha^{-1} and >200 kg N ha^{-1}) were compared to the needle samples collected from unfertilized plots (Table 1). A closer examination of the continuum-removed reflectance spectra and the distributions of AUC for the fourth absorption feature confirmed that samples collected from fertilized and unfertilized plots differed for current-year needles, whereas no difference was observed for previous-year needles (Fig. 5). The distributions of AUC values in the fourth absorption feature were similar between current-year needle samples collected from moderate and high fertilization intensity plots, even though both differed from the samples collected from the unfertilized plots (Fig. 5).

3.1.3. Nutrient contents and morphological properties of needles

The differences in the nutrient contents and morphological properties between needle samples collected from fertilized and unfertilized plots were small in both current-year and previous-year needles (Table 2). These were often attributed to the narrow ranges in nutrient contents and morphological properties (Table 2). The differences between needle age cohorts were larger than differences between fertilization treatments (Table 2).

The needle samples collected from fertilized plots had slightly lower median SLA compared to unfertilized plots for both current-year and previous-year needles (Table 2). SLA showed a decreasing trend with increasing fertilization intensity across both needle age groups (Fig. 6A). A statistically significant difference in SLA was found between the current-year needle samples collected from plots with high fertilization intensity (>200 kg N ha^{-1}) and from unfertilized plots (Fig. 6A). No statistically significant differences were found for WC between needle samples collected from fertilized and unfertilized plots, while previous-year needles had marginally lower WC values than current-year needles (Fig. 6B, Table 2).

Needle N and K content were similar between samples collected from fertilized and unfertilized plots across both needle age cohorts (Table 2, Fig. 6C, Fig. 6E). Previous-year needles tended to have lower P and K content compared to current-year needles (Table 2, Fig. 6D, Fig. 6E). Both current-year and previous-year needle samples showed a decreasing trend in P and K content with increasing fertilization intensity (Fig. 6D, Fig. 6E). Previous-year needle samples collected from high fertilization intensity plots showed statistically significant difference in P content compared to the previous-year samples collected from unfertilized plots (Fig. 6D). B content exhibited statistically significant differences between needle samples collected from unfertilized and fertilized plots across both needle age cohorts, with higher fertilization intensity leading to significantly higher B content (Table 2, Fig. 6F). For further details on the other biochemical properties measured, see Appendix B.

3.2. Spectral classification of needle samples collected from fertilized and unfertilized plots

Statistical analyses showed that the spectra of current-year needle samples were different in needle samples collected from fertilized and unfertilized plots (Table 1 and Fig. 5). Due to minimal spectral differences between needle samples from moderate and high fertilization intensity plots, a binary classification between needle samples collected from fertilized (combined) and unfertilized plots was conducted. The best model performance was achieved using AUC values from the fourth continuum-removed absorption feature (1112–1272 nm, Fig. 5), outperforming other tested input feature sets, including the full-range and continuum-removed reflectance, transmittance, and albedo spectra (results not shown). The needle samples collected from fertilized plots exhibited stronger classification performance, with a PA of 83.3 %, UA of 90.9 %, and an F1-score of 87.0 %, indicating that most predicted current-year needle samples collected from fertilized plots were correctly classified. In contrast, the needle samples collected from unfertilized plots had the same PA of 83.3 %, but a lower UA (71.4 %) and F1-score (76.9 %), highlighting more frequent misclassifications. Despite this, the model demonstrated a good ability to classify both needle sample classes (BA of 83.3 %). This result suggests a consistent differentiation between current-year needle samples collected from fertilized and unfertilized plots.

3.3. Estimating morphological properties and nutrient contents from needle spectra

Needle morphological properties and nutrient contents were better predicted using the reflectance spectra as input feature than the albedo spectra (Table 3). However, both input features struggled to predict nutrient contents, while performing well for SLA and WC (Table 3). Using reflectance spectra, SLA and WC showed moderate-to-good generalization (R^2 values of 0.7 and 0.8, respectively) with low-to-

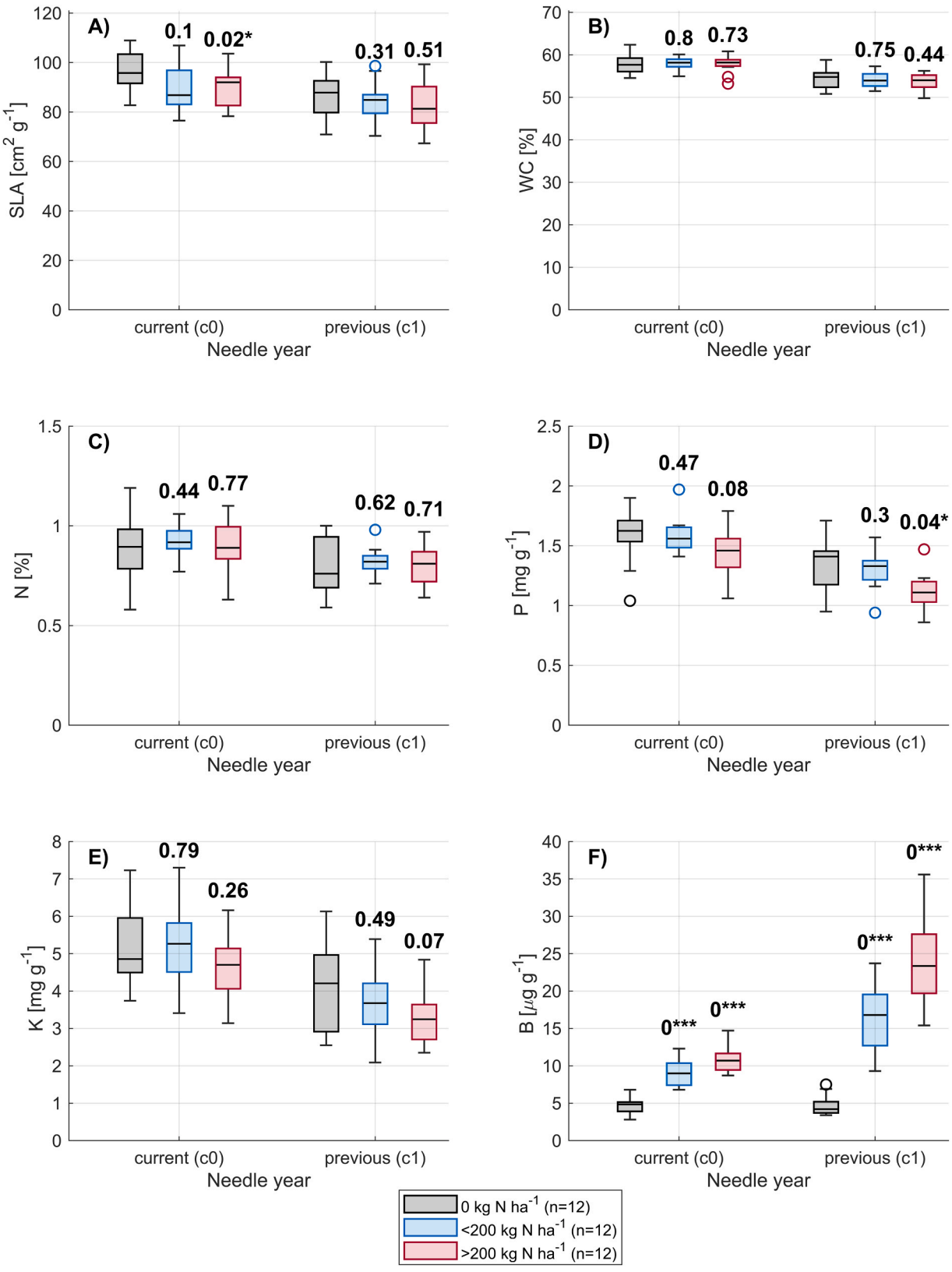

Fig. 6. Morphological properties and nutrient contents of current-year (c0) and previous-year (c1) needles of Norway spruce. The bars correspond to three different levels of fertilization intensity. A) specific leaf area, B) water content, C) nitrogen, D) phosphorus, E) potassium, and F) boron content. The values above the box-and-whisker plots indicate the p-value of the Mann-Whitney *U* test when comparing each of the fertilized groups against the unfertilized group (* $p < 0.05$, ** $p < 0.01$, *** $p < 0.001$).

Table 3
Results for partial least squares regression (PLSR) models predicting morphological properties and nutrient contents of needles using reflectance or albedo spectra as input features. Abbreviations: RMSEP (root mean square error of prediction), RMSEP-% (relative RMSEP), R^2 (out-of-sample coefficient of determination), and $CI_{0.95}$ (95 % confidence interval for error estimates). "Modal no. components" refers to the most frequently selected number of components for each needle property during the nested cross-validation procedure.

	All needle samples (c0 + c1, n = 72)							
	Input: Reflectance				Input: Albedo			
Needle property	RMSEP ($CI_{0.95}$)	RMSEP-% ($CI_{0.95}$)	R^2	Modal no. components	RMSEP ($CI_{0.95}$)	RMSEP-% ($CI_{0.95}$)	R^2	Modal no. components
SLA [$cm^2\ g^{-1}$]	5.5 (4.2–6.5)	6.2 (4.8–7.4)	0.7	5	5.6 (4.6–6.5)	6.4 (5.2–7.4)	0.7	5
WC [%]	1.2 (0.8–1.5)	2.2 (1.5–2.8)	0.8	10	1.3 (1.0–1.5)	2.3 (1.7–2.8)	0.8	6
Nitrogen, **N** [%]	0.1 (0.0–0.1)	9.7 (4.8–12.9)	0.5	12	0.1 (0.1–0.1)	11.4 (9.3–13.1)	0.3	12
Carbon, **C** [%]	0.5 (0.4–0.6)	1.0 (0.8–1.2)	0.1	8	0.5 (0.3–0.6)	0.9 (0.7–1.1)	0.1	12
Potassium, **K** [mg g^{-1}]	1.0 (0.7–1.3)	23.6 (16.0–29.4)	0.2	5	1.1 (0.8–1.3)	24.9 (19.1–29.6)	0.1	10
Phosphorus, **P** [mg g^{-1}]	0.2 (0.1–0.3)	14.5 (10.0–17.8)	0.3	10	0.2 (0.2–0.3)	15.6 (11.6–18.7)	0.2	7
Aluminum, **Al** [µg g^{-1}]	18.8 (11.0–24.2)	46.8 (27.4–60.2)	0.3	5	19.4 (12.0–24.6)	48.3 (30.0–61.4)	0.2	6
Boron, **B** [µg g^{-1}]	6.9 (4.8–8.5)	59.9 (41.7–73.7)	0.1	5	7.0 (5.6–8.2)	60.2 (48.0–70.4)	0.1	7
Calcium, **Ca** [µg g^{-1}]	1901.8 (869.4–2545.2)	43.1 (19.7–57.7)	0.3	5	1751.2 (919.3–2300.0)	39.7 (20.8–52.1)	0.5	6
Copper, **Cu** [µg g^{-1}]	2.9 (0.0–4.7)	103.1 (0.0–165.8)	−0.0	1	3.0 (0.0–4.8)	108.3 (0.0–171.4)	−0.2	1
Iron, **Fe** [µg g^{-1}]	3.5 (2.8–4.1)	16.5 (13.0–19.4)	0.3	5	3.8 (3.0–4.4)	17.8 (14.1–20.8)	0.1	2
Magnesium, **Mg** [µg g^{-1}]	196.2 (158.9–227.5)	20.8 (16.8–24.1)	0.0	4	194.2 (141.4–235.4)	20.6 (15.0–25.0)	0.1	3
Manganese, **Mn** [µg g^{-1}]	421.5 (277.8–527.4)	57.9 (38.2–72.5)	0.3	2	411.9 (206.2–544.7)	56.6 (28.3–74.8)	0.3	4
Sulphur, **S** [µg g^{-1}]	59.9 (38.4–75.5)	8.6 (5.5–10.8)	0.4	6	59.9 (41.2–74.1)	8.6 (5.9–10.6)	0.4	5
Zinc, **Zn** [µg g^{-1}]	6.7 (4.0–8.5)	29.1 (17.5–37.3)	0.3	5	7.0 (4.7–8.6)	30.4 (20.5–37.7)	0.2	8

very-low RMSEP-% values (6.2 % and 2.2 %, respectively) and narrow confidence intervals (4.8–7.4 % and 1.5–2.8 %, respectively) (Fig. 7A and B). For N, the predictive capability was moderate ($R^2 = 0.5$) but had a higher RMSEP-% (9.7 %) and some instability in its (i.e., wider) confidence intervals (4.8–12.9 %) (Fig. 7C). In contrast, P, K, and the essential micronutrient B had poor predictability (Fig. 7D–F). Despite variability in accuracies across predicted morphological properties and nutrient contents, stable numbers of components were consistently selected to the models, and the 95 % confidence intervals around mean point estimates remained narrow (Fig. 7).

Next, we used mean PLSR VIP scores greater than 1 to identify the most influential spectral regions in our nested cross-validation procedure (Fig. 8). For reference, we compared these key wavelengths to known spectral absorption features associated with various foliar chemical constituents, including chlorophylls, carotenoids, anthocyanins, phenolic compounds, water, proteins, oils, starches, lignin, cellulose, sugars, and nitrogen (Fig. 8D). In general, the highest VIP scores (>1) revealed distinct peak wavelength regions that contributed significantly to estimating both morphological properties and nutrient contents with PLSR. Most peak importances were concentrated in the VIS and SWIR regions (Figs. 8B and 8C). For morphological properties, peak contributions aligned with known absorption wavelengths around 430, 449, 453, 475, 700, 1420, 1660, and 1690 nm (Fig. 8B). Many of these wavelengths were also important for nutrient contents, with additional clear peaks for nitrogen near 520, 642, 1820, 1940, 1980, 2000, and 2080 nm (Fig. 8C).

Although both morphological properties and nutrient contents of needles shared key spectral regions, nutrient contents exhibited more distinct peaks, especially between the green peak and red-edge region and toward the end of the SWIR (Fig. 8C). Interestingly, no VIP score peaks above 1 were detected between the 910 and 1200 nm features for either morphological properties or nutrient contents, nor between the 1450 and 1540 nm features for nutrient contents (Fig. 8B and C). For morphological properties, absorption features near 642–680 nm, 1820 nm, 1940–2000 nm, 2080–2100 nm, and 2180 nm were not identified as most important or influential for the estimations using PLSR (Fig. 8B).

4. Discussion

4.1. Effects of nitrogen fertilization on the spectral properties of needles

In Nordic countries, the typical N fertilizer dose applied in Norway spruce stands is 150 kg N ha^{-1} (Äijälä et al., 2019; Hedwall et al., 2014). Nitrogen fertilization has been shown to increase the growing stock volume 6–20 m^3 ha^{-1} during 8–10 years in mesic mineral soil sites (Kukkola and Saramäki, 1983; Nohrstedt, 2001; Saarsalmi and Mälkönen, 2001; Bergh et al., 2014). The strongest increase in annual volume growth occurs within 3–5 years after fertilization (Kukkola and Saramäki, 1983; Ilvesniemi et al., 2023). Higher N doses exceeding 150 kg N ha^{-1} have been shown to yield diminishing returns in terms of additional growth response (Ilvesniemi et al., 2023). In comparison, our measurements showed that both moderate (<200 kg N ha^{-1}) and high N fertilizer dose had a small effect (<3 % across the 400 – 2500 nm range) on needle spectral properties five years after fertilization. The results suggest a saturation in the spectral changes beyond moderate levels of N fertilization, consistent with findings reported for volume growth, and for spectral properties of Engelmann spruce seedlings (Moran et al., 2000).

Regarding the magnitude of spectral changes, a previous study by

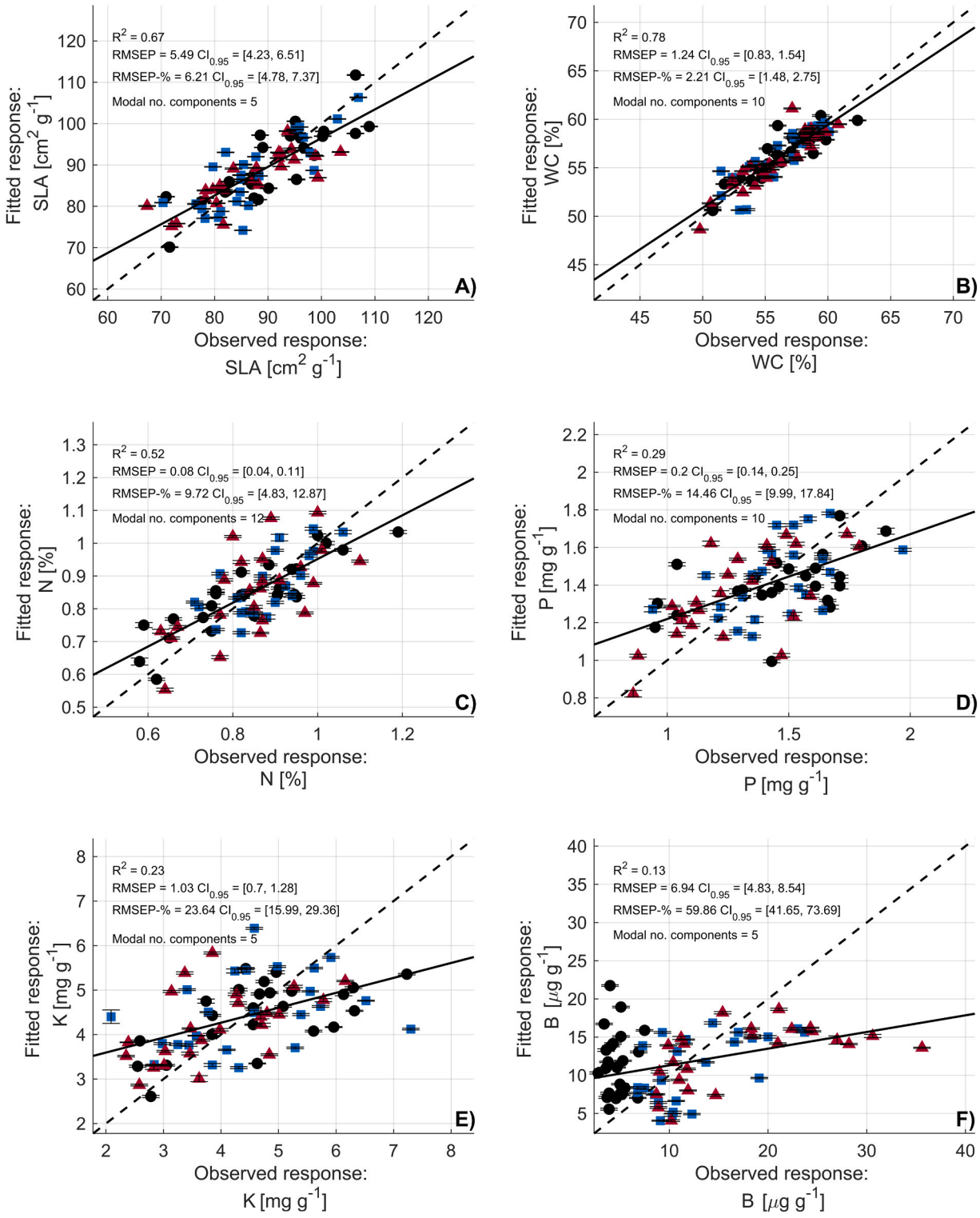

Fig. 7. Results for partial least squares regression (PLSR) models predicting A) specific leaf area, B) water content, C) nitrogen, D) phosphorus, E) potassium, and F) boron content of needles. Error bars denote the 95 % confidence intervals for each fitted response value. The black dashed line shows the 1:1 line, and the black solid line shows the regression line. Abbreviations: RMSEP (root mean square error of prediction), RMSEP-% (relative RMSEP), R^2 (out-of-sample coefficient of determination), and $CI_{0.95}$ (95 % confidence interval for error estimates). "Modal no. components" refers to the most frequently selected number of components for each needle property. The black circles, blue squares, and red triangles denote the needle samples collected from unfertilized (control) and fertilized plots that received 0 kg N ha^{-1}, < 200 kg N ha^{-1}, and > 200 kg N ha^{-1} fertilization, respectively.

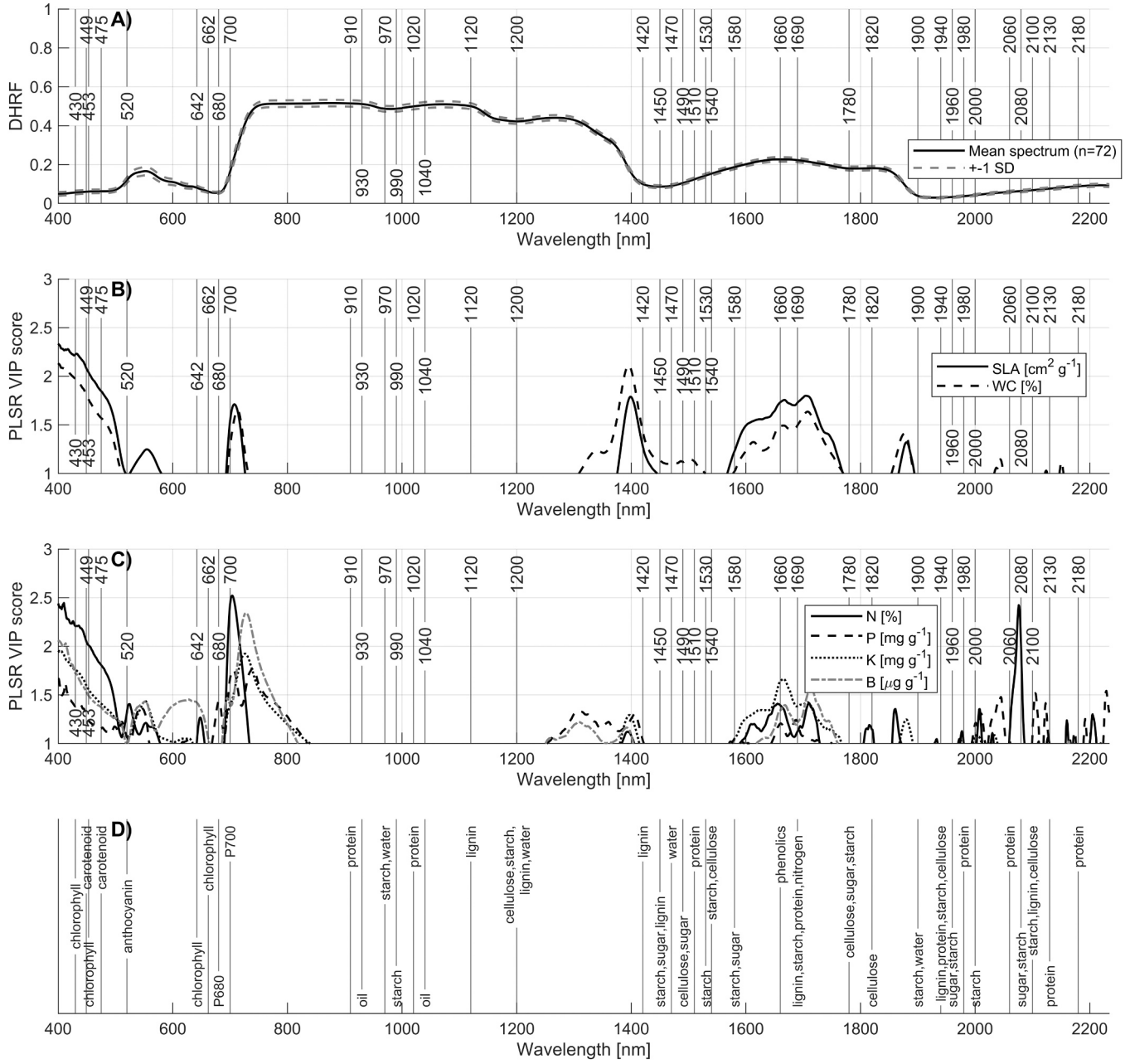

Fig. 8. A) Mean reflectance spectrum of Norway spruce needles with absorption features (vertical black lines) in the visible to short-wave infrared that have been related to foliar chemical concentrations (D) (Ziechmann, 1964; Curran, 1989; Elvidge, 1990; McLellan et al., 1991a, 1991b; Ben-Dor et al., 1997; Ribeiro da Luz, 2006; Ribeiro da Luz and Crowley, 2007; Ustin et al., 2009; Coward, 2010; Agarwal and Atalla, 2010; Kokaly and Skidmore, 2015), B) the PLSR variable importance in projection (VIP) scores for two needle morphological properties: specific leaf area (SLA) and water content (WC), and C) the PLSR VIP scores for nitrogen (N), phosphorus (P), potassium (K), and boron (B).

Hovi et al. (2022a) also reported small maximum spectral differences (<3.3 % at 490 nm, <13 % at 560 nm, <3.7 % at 665 nm, and <14.4 % at 865 nm) in current-year and previous-year needles from different study areas, albeit with mean differences slightly larger than those in our study. Notably, we found statistically significant differences of reflectance, transmittance, and albedo spectra between the needles collected from unfertilized and fertilized plots only in current-year needles (Fig. 3, Fig. 5, and Table 1). The spectral differences being observed only in current-year needles could be due to their active involvement in growth and nutrient uptake, which makes them more responsive to fertilization and more likely to show detectable spectral changes (Nambiar and Fife, 1987). This aligns with evidence that, e.g., SLA responds to N most strongly during early leaf expansion, influencing both structure and biochemistry, and consequently, optical properties (Reich et al., 1991).

While N fertilization did affect some nutrient contents of needles (Fig. 6, Fig. B.1, Fig. B.2, and Table 2), the changes were either too small to create clear spectral differences or involved nutrients without specific absorption features (e.g., B). Overall, our results highlight that the Norway spruce needle spectral properties, nutrient contents, and morphological properties differ more between needle age cohorts than between different fertilization levels (Table 2). The latter aligns with earlier literature that shows a small or modest effect of site soil conditions (Lhotáková et al., 2021) or climate (Wright et al., 2004) on leaf traits, including their spectral properties.

Our results highlight that the absorption feature centered around 1200 nm has clear potential to differentiate between the current-year needles collected from fertilized and unfertilized plots (Fig. 5 and Table 1). While a single wavelength region is rarely tied to a single constituent, Curran (1989) identified the 1200 nm feature as part of the absorption spectra of water, cellulose, sugar, starch, and lignin (Fig. 8). As this wavelength range exhibits minimal pigment absorption, the changes in the internal needle structure become more pronounced than in other wavelength regions (Sims and Gamon, 2002). In addition, at high WC, the major water absorption bands (1450 nm, 1940 nm, and 2500 nm) can become saturated, making the intermediate (1650 nm and 2200 nm) and weaker bands (970 nm and 1200 nm) more sensitive to differences in WC and interactions with other needle constituents (Gao, 1996). SLA also differed specifically in the current-year needle samples collected from high fertilization intensity plots vs. unfertilized plots (Fig. 6) and could partially explain why the NIR absorption feature at 1200 nm worked for detecting the effect of N fertilization. Thus, our interpretation is that fertilization-induced changes in the properties of current-year needles in peak growing season are complex, with N fertilization effects most clearly observable in the NIR region, highlighting differences in internal needle structure.

Our results indicated that reflectance performed the best out of the three spectral variables when used in classifying current-year needle samples between unfertilized and fertilized plots (Fig. 5 and Table 1), and in estimating nutrient content and morphological properties (Fig. 7 and Table 3). It should be noted that when using integrating spheres to measure needle samples with gaps, the reflectance and transmittance measurements are linked since both contain surface and interior scattering components. In contrast, for flat leaves that fully cover the measurement area, these two variables are more distinctly separated, as photons cannot scatter from individual needle surfaces and pass through the gaps between them. In addition, the correction for gap fraction in a needle sample is challenging for transmittance measurements made in VIS and SWIR regions, where the needle transmittance is low and the illumination passing through the gaps has a large contribution to the measurements (Hovi et al., 2022a). These reasons may explain why needle reflectance outperformed both transmittance and albedo spectra.

Measuring needle samples with integrating spheres is laborious, limiting the sample sizes used in the statistical analysis and modeling in our study. The accurate measurements using an integrating sphere, however, facilitate a comprehensive analysis of the effects of N fertilization on the spectral properties of needles, and our study provides currently the largest dataset and analysis of the fertilization effects on coniferous needle spectra conducted on mature trees. Hence, our measurements and results contribute to a better understanding of the effects of N fertilization treatments on needle spectra of Norway spruce forests. It should be emphasized that, because of the applied sampling design, our results are most representative of dominant trees. In addition, further studies in other locations, climates, and across tree species are necessary to assess the generality of our findings.

4.2. *Implications for developing remote sensing for assessing nitrogen fertilization in forests*

Successful application of remote sensing to reveal whether a certain forest stand should be, or has already been fertilized, would transform the ability to plan forest fertilization in practice, and contribute to improved economic and environmental performance of boreal forestry. In an ideal situation, aerial imaging spectroscopy (i.e., hyperspectral data) could facilitate the assessment of fertilization need, and provide foundation to plan a fertilization scheme (i.e., the fertilizer dose and type) to fulfill the actual nutrient demand of the forest stand, or even individual trees. Our classification test showed that needle samples from fertilized and unfertilized plots could be separated based on their spectral properties. This separation could be done even with the small spectral differences, when restricting the analysis to current-year needles. We consider the detectability reasonable because, e.g., chlorophyll fluorescence emission is low relative to leaf reflectance (2–3 % in the red and NIR regions) (Zarco-Tejada et al., 2012) yet its signal in vegetation can be extracted from remote sensing data (e.g., Guanter et al., 2007).

Our needle-level results cannot, however, be directly applied at a tree or canopy scale as there the signal is confounded by the interplay between tree and canopy structure and the complex scattering and emission processes. Factors such as illumination and observation angles (Kuusk et al., 2014), leaf angle distributions and clumping (Asner, 1998; Béland and Kobayashi, 2024), spatial distribution of canopy elements (Halme and Mõttus, 2023), surrounding environment (Hase et al., 2022), and multiple scattering (Rautiainen and Stenberg, 2005) influence the canopy reflectance spectra, and must be considered when retrieving spectral features that may show the effects of N fertilization on trees from optical remote-sensing data. Also, needle age was identified as a key factor that should be accounted for when upscaling to tree and canopy scale.

While our exploratory classification was inherently challenging due to the needle- or shoot-level spatial resolution and limited sample size, these constraints highlight the potential value of remote sensing techniques that could help overcome sampling limitations. Since the observable changes were detected at the needle-level, applying remote sensing could facilitate a more comprehensive assessment of samples from the canopy and enable the detection of even subtle differences in mean spectral properties. However, detecting these differences would warrant ultra-high spatial resolution imaging spectroscopy, which enables identifying within-crown features, both with needle- or shoot-level precision. In addition to evaluating the potential of detecting fertilization status from hyperspectral remote sensing data, our study identified the most influential wavelength regions for estimation of biochemical and morphological traits of Norway spruce needles. The most influential wavelength regions of the spectrum for retrieving needle biochemical and morphological traits were mostly concentrated in VIS and SWIR regions, with consistent patterns across the different nutrient contents

and morphological properties. Interestingly, the influential peaks in our study (430–475, 642, 700, 1420, 1660–1690, 1940–1980, 2000–2080 nm) closely resemble the VIP score peaks of previous studies, even with global datasets (e.g., Ji et al., 2024). Our results also suggest that the common VIP score peak regions across measured traits in the VIS region could be attributed to chlorophyll and carotenoid (i.e., pigment) content, and in the SWIR region to lignin, starch, protein, and sugar (i.e., structural and metabolic compounds) content.

To enhance the interpretation of remotely sensed data for precision fertilization of boreal forests, we recommend future research should: 1) test whether the NIR absorption feature centered around 1200 nm persists when scaling up from the needle-level to entire coniferous forest canopies, 2) develop image processing algorithms capable of detecting small needle-level spectral changes induced by fertilization using hyperspectral data, and 3) explore how and to which extent structural differences between fertilized and unfertilized stands, jointly with the retrieved needle-level spectra, could be utilized to assess the fertilization requirements.

5. Conclusions

In this extensive pilot study, we conducted spectral, nutrient content, and morphological measurements of needles from a unique controlled fertilization experiment of mature Norway spruce stands. We found that N fertilization has a small yet detectable effect on the spectral properties of current-year needles. Our results suggest that the spectral changes saturate beyond moderate levels of N fertilization, with significant differences observed exclusively in current-year needle samples. Using continuum removal for spectral feature analysis, we found that the absorption feature centered around 1200 nm, reflecting mainly morphological and structural differences, showed the highest potential in differentiating current-year needles collected from fertilized and unfertilized plots. Developing remote sensing applications for assessing fertilization needs and developing precision fertilization schemes in boreal forests could both help to decrease adverse environmental effects and increase cost-efficiency and resource-efficiency of fertilization.

CRediT authorship contribution statement

Aarne Hovi: Writing – review & editing, Supervision, Software, Project administration, Methodology, Investigation, Funding acquisition, Data curation, Conceptualization. **Samuli Launiainen:** Writing – review & editing, Resources, Methodology, Funding acquisition, Conceptualization. **Heli Peltola:** Writing – review & editing, Resources, Methodology, Funding acquisition, Conceptualization. **Miina Rautiainen:** Writing – review & editing, Supervision, Resources, Methodology, Funding acquisition, Conceptualization. **Jussi Juola:** Writing – original draft, Visualization, Software, Methodology, Investigation, Formal analysis, Data curation, Conceptualization.

Declaration of Competing Interest

The authors declare that they have no known competing financial interests or personal relationships that could have appeared to influence the work reported in this paper.

Acknowledgements

We would like to thank Risto Ikonen (UEF) and Jaan Rönkkö (Aalto University) for significant contributions in field work. Thanks also to Leena Kuusisto and Olli Muhonen at UEF, and Jere Kaivosoja and the staff of LUKE's Savonlinna research infrastructure for the support provided for this research.

This study was mainly funded by The Foundation for Research of Natural Resources in Finland. Tornator, Yara, ForestVital, University of Eastern Finland (UEF) and the Research Council of Finland [the SRC FORBIO project, decision number 314224; PREFER, decision numbers 348096 (UEF) and 348102 (Luke); the UNITE flagship, decision numbers 337127, 357906 and 359172], are acknowledged for support for establishing fertilization experiment and conducting field (tree and stand attributes) measurements and nutrient analyses of needles and soil in years 2018–2024. This study also received funding from the European Research Council (ERC) under the European Union's Horizon 2020 research and innovation programme [grant agreement No 771049/Rautiainen]. The text reflects only the authors' view and the Agency is not responsible for any use that may be made of the information it contains.

Appendix A

Table A.1
Wavelength ranges of the left and right continuum endpoints used to calculate the area under the curve (AUC) for the seven major absorption regions in the 400–2500 nm range for reflectance, transmittance, and albedo spectra

	Reflectance [DHRF]		Transmittance [DHTF]		Albedo	
	Left continuum endpoint	Right continuum endpoint	Left continuum endpoint	Right continuum endpoint	Left continuum endpoint	Right continuum endpoint
Absorption region	Wavelength range of endpoints [nm]	Wavelength range of endpoints [nm]	Wavelength range of endpoints [nm]	Wavelength range of endpoints [nm]	Wavelength range of endpoints [nm]	Wavelength range of endpoints [nm]
1	400	536–547	400	536–550	400	536–548
2	552–553	743–750	553–554	744–752	552–554	743–751
3	880–895	1063–1078	888–913	1068–1080	882–899	1068–1078
4	1113–1117	1265–1270	1112–1117	1267–1272	1114–1116	1266–1271
5	1289–1297	1650–1672	1288–1294	1651–1677	1289–1295	1651–1675
6	1681–1698	1804–1829	1683–1706	1813–1830	1684–1708	1801–1830
7	1827–1836	2199–2231	1826–1838	2184–2234	1828–1835	2200–2230

Appendix B

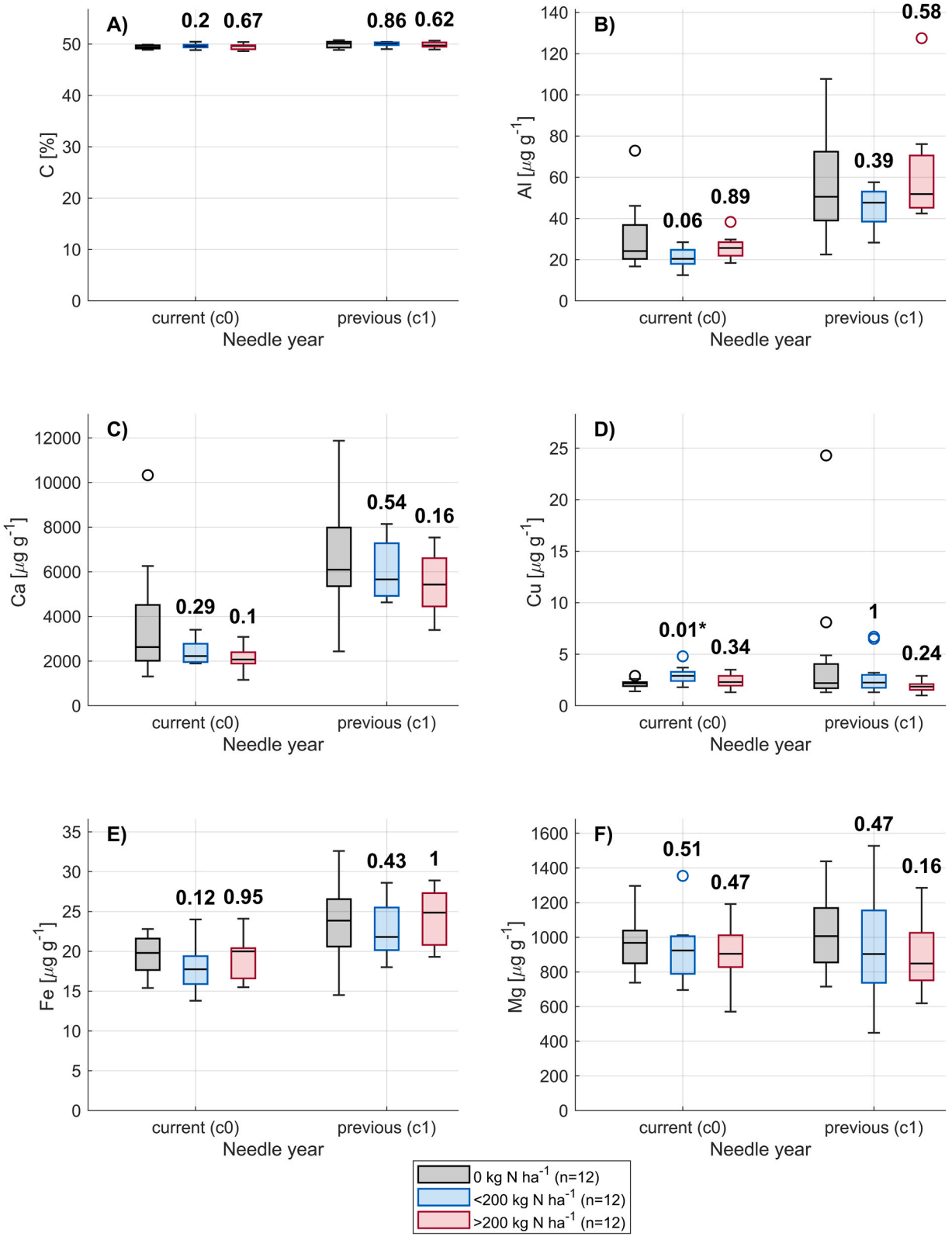

Fig. B.1. Needle nutrient contents of current-year (c0) and previous-year (c1) needles of Norway spruce. The bars correspond to three different levels of fertilization intensity. A) carbon, B) aluminum, C) calcium, D) copper, E) iron, and F) magnesium content. The values above the box-and-whisker plots indicate the p-value of the Mann-Whitney *U* test when comparing each of the fertilized groups against the unfertilized group (* $p < 0.05$)

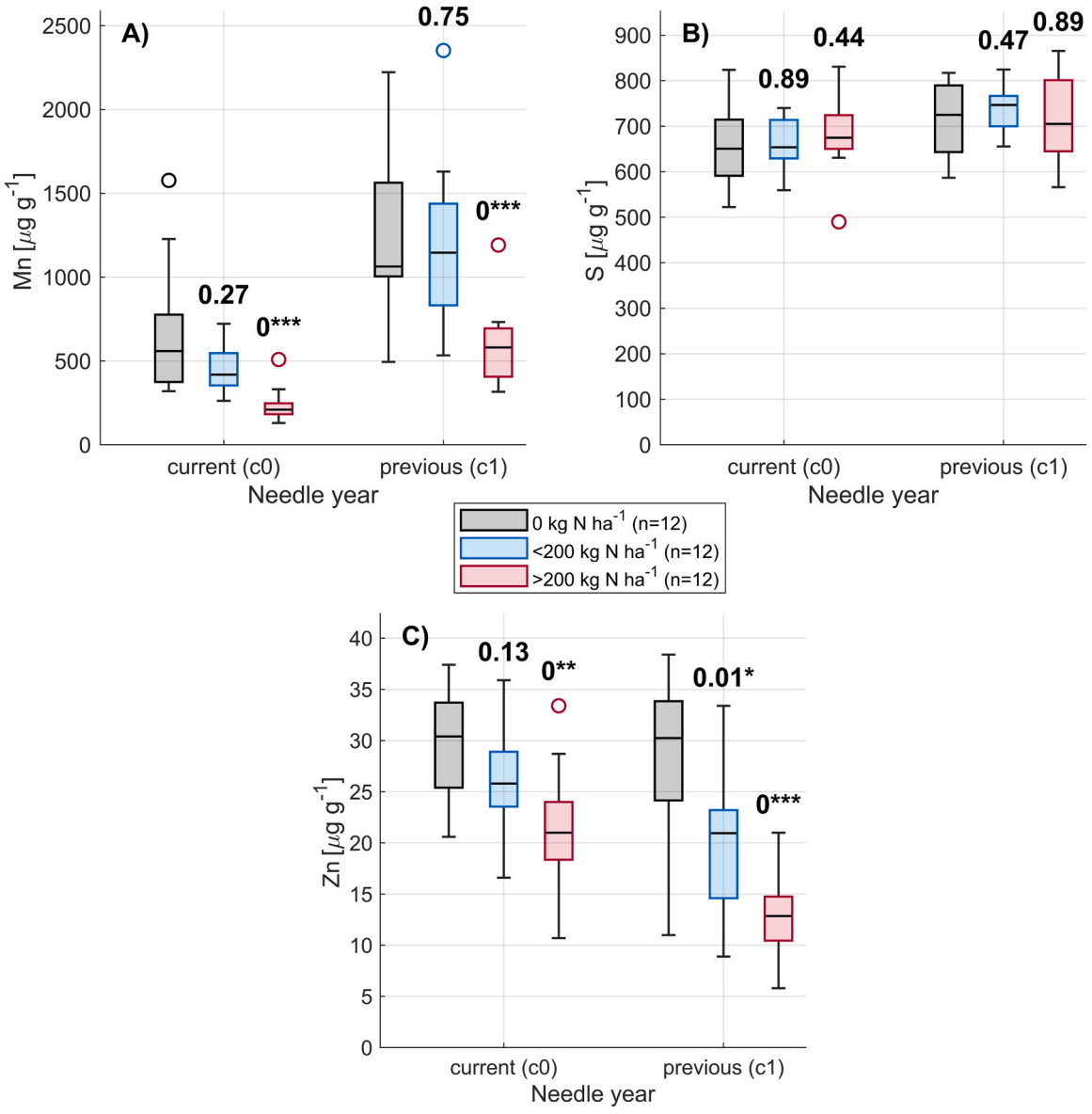

Fig. B.2. Needle nutrient contents of current-year (c0) and previous-year (c1) needles of Norway spruce. The bars correspond to three different levels of fertilization intensity. A) manganese, B) sulfur, and C) zinc content. The values above the box-and-whisker plots indicate the p-value of the Mann-Whitney *U* test when comparing each of the fertilized groups against the unfertilized group (* $p < 0.05$, ** $p < 0.01$, *** $p < 0.001$)

Data availability

Data will be made available on request.

References

Agarwal, U.P., Atalla, R.H., 2010. Vibrational spectroscopy. In: Heitner, C., Dimmel, D. R., Schmidt, J.A. (Eds.), Lignin and Lignans Advances In Chemistry. CRC Press, Boca Raton, FL. Chapter 4: 103-136: ISBN: 9781574444865.

Äijälä, O., Koistinen, A., Sved, J., Vanhatalo, K., Väisänen, P., 2019. Metsänhoidon suositukset- METSÄNHOITO. [Finnish forest management recommendations]. Metsätalouden kehittämiskeskus Tapion julkaisuja. 252 p. ISBN 978-952-5632-75-0.

Asner, G.P., 1998. Biophysical and biochemical sources of variability in canopy reflectance. Remote Sens. Environ. https://doi.org/10.1016/S0034-4257(98)00014-5.

Bates, S., Hastie, T., Tibshirani, R., 2024. Cross-Validation: what does it estimate and how well does it do it? J. Am. Stat. Assoc. 119. https://doi.org/10.1080/01621459.2023.2197686.

Béland, M., Kobayashi, H., 2024. Drivers of deciduous forest near-infrared reflectance: a 3D radiative transfer modeling exercise based on ground lidar. Remote Sens. Environ. 302. https://doi.org/10.1016/j.rse.2023.113951.

Ben-Dor, E., Inbar, Y., Chen, Y., 1997. The reflectance spectra of organic matter in the visible near-infrared and short wave infrared region (400–2500 nm) during a controlled decomposition process. Remote Sens. Environ. 61. https://doi.org/10.1016/S0034-4257(96)00120-4.

Bergh, J., Nilsson, U., Allen, H.L., Johansson, U., Fahlvik, N., 2014. Long-term responses of Scots pine and Norway spruce stands in Sweden to repeated fertilization and thinning. Ecol. Manag. 320. https://doi.org/10.1016/j.foreco.2014.02.016.

Boeraeve, M., Granath, G., Lindahl, B.D., Clemmensen, K.E., Strengbom, J., 2025. How does forest fertilization influence tree productivity of boreal forests? An analysis of data from commercial forestry across Sweden. J. Environ. Manag. 373. https://doi.org/10.1016/j.jenvman.2024.124023.

Bonan, G.B., 2008. Forests and climate change: forcings, feedbacks, and the climate benefits of forests. Science 1979. https://doi.org/10.1126/science.1155121.

Brereton, R.G., Lloyd, G.R., 2010. Support vector machines for classification and regression. Analyst. https://doi.org/10.1039/b918972f.

Burnett, A.C., Anderson, J., Davidson, K.J., Ely, K.S., Lamour, J., Li, Q., Morrison, B.D., Yang, D., Rogers, A., Serbin, S.P., 2021. A best-practice guide to predicting plant traits from leaf-level hyperspectral data using partial least squares regression. J. Exp. Bot. 72. https://doi.org/10.1093/jxb/erab295.

Cajander, A., 1949. Forest types and their significance. Acta For. Fenn. 56. https://doi.org/10.14214/aff.7396.

Chandler, J.W., Dale, J.E., 1995. Nitrogen deficiency and fertilization effects on needle growth and photosynthesis in sitka spruce (Picea sitchensis). Tree Physiol. 15. https://doi.org/10.1093/treephys/15.12.813.
Chong, I.G., Jun, C.H., 2005. Performance of some variable selection methods when multicollinearity is present. Chemom. Intell. Lab. Syst. 78. https://doi.org/10.1016/j.chemolab.2004.12.011.
Clark, R.N., Roush, T.L., 1984. Reflectance spectroscopy: quantitative analysis techniques for remote sensing applications. J. Geophys Res. 89. https://doi.org/10.1029/JB089iB07p06329.
Coward, J.L., 2010. FTIR spectroscopy of synthesized racemic nonacosan-10-ol: a model compound for plant epicuticular waxes. J. Biol. Phys. 36. https://doi.org/10.1007/s10867-010-9192-6.
Curran, P.J., 1989. Remote sensing of foliar chemistry. Remote Sens. Environ. https://doi.org/10.1016/0034-4257(89)90069-2.
Elvidge, C.D., 1990. Visible and near infrared reflectance characteristics of dry plant materials. Int. J. Remote Sens. https://doi.org/10.1080/01431169008955129.
Eriksson, L., Byrne, T., Johansson, E., Trygg, J., Vikström, C., 2013. Multi- and megavariate data analysis basic principles and applications. Technometrics. https://doi.org/10.1198/tech.2003.s162.
Field, C., Mooney, H.A., 1986. The photosynthesis-nitrogen relationship in wild plants. In: Givnish, T.J. (Ed.), On the Economy of Plant Form and Function. Cambridge University Press, pp. 25–55.
Gao, B.C., 1996. NDWI - a normalized difference water index for remote sensing of vegetation liquid water from space. Remote Sens. Environ. 58. https://doi.org/10.1016/S0034-4257(96)00067-3.
Gosselin, R., Rodrigue, D., Duchesne, C., 2010. A Bootstrap-VIP approach for selecting wavelength intervals in spectral imaging applications. Chemom. Intell. Lab. Syst. 100. https://doi.org/10.1016/j.chemolab.2009.09.005.
Guanter, L., Alonso, L., Gómez-Chova, L., Amorós-López, J., Vila, J., Moreno, J., 2007. Estimation of solar-induced vegetation fluorescence from space measurements. Geophys Res. Lett. 34. https://doi.org/10.1029/2007GL029289.
Haaland, D.M., Thomas, E.V., 1988. Partial Least-Squares methods for spectral analyses. 1. relation to other quantitative calibration methods and the extraction of qualitative information. Anal. Chem. 60. https://doi.org/10.1021/ac00162a020.
Håkansson, C., Hedwall, P.O., Strömgren, M., Axelsson, M., Bergh, J., 2021. Effects of fertilization on soil CH4 and N2O fluxes in young Norway spruce stands. Ecol. Manag. 499. https://doi.org/10.1016/j.foreco.2021.119610.
Halme, E., Mõttus, M., 2023. Improved parametrisation of a physically-based forest reflectance model for retrieval of boreal forest structural properties. Silva Fenn. 57. https://doi.org/10.14214/sf.22028.
Hase, N., Doktor, D., Rebmann, C., Dechant, B., Mollenhauer, H., Cuntz, M., 2022. Identifying the main drivers of the seasonal decline of near-infrared reflectance of a temperate deciduous forest. Agric. Meteor. 313. https://doi.org/10.1016/j.agrformet.2021.108746.
Hastie, T., Tibshirani, R., Friedman, J., 2009. Elements of statistical learning, second ed., Elements. Springer. https://doi.org/10.1007/978-0-387-84858-7.
Hedwall, P.O., Gong, P., Ingerslev, M., Bergh, J., 2014. Fertilization in Northern forests - biological, economic and environmental constraints and possibilities. Scand. J. Res. https://doi.org/10.1080/02827581.2014.926096.
Heimann, M., Reichstein, M., 2008. Terrestrial ecosystem carbon dynamics and climate feedbacks. Nature. https://doi.org/10.1038/nature06591.
Homolová, L., Lukeš, P., Malenovský, Z., Lhotáková, Z., Kaplan, V., Hanuš, J., 2013. Measurement methods and variability assessment of the Norway spruce total leaf area: implications for remote sensing. Trees Struct. Funct. 27. https://doi.org/10.1007/s00468-012-0774-8.
Hovi, A., Forsström, P., Mõttus, M., Rautiainen, M., 2018. Evaluation of accuracy and practical applicability of methods for measuring leaf reflectance and transmittance spectra. Remote Sens. 10. https://doi.org/10.3390/rs10010025.
Hovi, A., Lukeš, P., Homolová, L., Juola, J., Rautiainen, M., 2022a. Small geographical variability observed in Norway spruce needle spectra across Europe. Silva Fenn. https://doi.org/10.14214/sf.10683.
Hovi, A., Mõttus, M., Juola, J., Manoocheri, F., Ikonen, E., Rautiainen, M., 2020. Evaluating the performance of a double integrating sphere in measurement of reflectance, transmittance, and albedo of coniferous needles. Silva Fenn. 54. https://doi.org/10.14214/sf.10270.
Hovi, A., Schraik, D., Hanuš, J., Homolová, L., Juola, J., Lang, M., Lukeš, P., Pisek, J., Rautiainen, M., 2022b. Assessment of a photon recollision probability based forest reflectance model in european boreal and temperate forests. Remote Sens Environ. 269. https://doi.org/10.1016/j.rse.2021.112804.
Huttunen, I., Huttunen, M., Salo, T., Mattila, P., Maanavilja, L., Silfver, T., 2023. National-scale nitrogen loading from the Finnish agricultural fields has decreased since the 1990s. Agric. Food Sci. 32. https://doi.org/10.23986/afsci.125385.
Hyvönen, R., Persson, T., Andersson, S., Olsson, B., Ågren, G.I., Linder, S., 2008. Impact of long-term nitrogen addition on carbon stocks in trees and soils in Northern Europe. Biogeochemistry 89. https://doi.org/10.1007/s10533-007-9121-3.
Ilvesniemi, H., Lehto, T., Smolander, A., Salminen, H., Kukkola, M., 2023. Puuston kasvuvasteet kivennäismailla. [Tree growth responses in mineral soils]. In Finnish In: Lehto T, Ilvesniemi H (Eds.) Metsänlannoitus nyt ja tulevaisuudessa: Synteesiraportti. Luonnonvara- ja biotalouden tutkimus 56/2023. Luonnonvarakeskus. Helsinki. s. 71–75.
Ji, F., Li, F., Hao, D., Shiklomanov, A.N., Yang, X., Townsend, P.A., Dashti, H., Nakaji, T., Kovach, K.R., Liu, H., Luo, M., Chen, M., 2024. Unveiling the transferability of PLSR models for leaf trait estimation: lessons from a comprehensive analysis with a novel global dataset. N. Phytol. 243. https://doi.org/10.1111/nph.19807.
Jokela, A., Bäck, J., Huttunen, S., Jalkanen, R., 1995. Excess nitrogen fertilization and the structure of Scots-pine needles. Eur. J. For. Pathol. 25. https://doi.org/10.1111/j.1439-0329.1995.tb00325.x.
Knyazikhin, Y., Schull, M.A., Stenberg, P., Mõttus, M., Rautiainen, M., Yang, Y., Marshak, A., Carmona, P.L., Kaufmann, R.K., Lewis, P., Disney, M.I., Vanderbilt, V., Davis, A.B., Baret, F., Jacquemoud, S., Lyapustin, A., Myneni, R.B., 2013. Hyperspectral remote sensing of foliar nitrogen content. Proc. Natl. Acad. Sci. 110. https://doi.org/10.1073/pnas.1210196109.
Kokaly, R.F., Skidmore, A.K., 2015. Plant phenolics and absorption features in vegetation reflectance spectra near 1.66 μm. Int. J. Appl. Earth Obs. Geoinf. 43. https://doi.org/10.1016/j.jag.2015.01.010.
Kukkola, M., Saramäki, J., 1983. Growth response in repeatedly fertilized pine and spruce stands on mineral soils. Commun. Inst. Fenn. 114, 55.
Kuusk, A., Kuusk, J., Lang, M., 2014. Measured spectral bidirectional reflection properties of three mature hemiboreal forests. Agric. Meteor. 185. https://doi.org/10.1016/j.agrformet.2013.10.011.
Lhotáková, Z., Kopačková-Strnadová, V., Oulehle, F., Homolová, L., Neuwirthová, E., Švik, M., Janoutová, R., Albrechtová, J., 2021. Foliage biophysical trait prediction from laboratory spectra in Norway spruce is more affected by needle age than by site soil conditions. Remote Sens. 13. https://doi.org/10.3390/rs13030391.
Lukeš, P., Stenberg, P., Rautiainen, M., Mõttus, M., Vanhatalo, K.M., 2013. Optical properties of leaves and needles for boreal tree species in Europe. Remote Sens. Lett. https://doi.org/10.1080/2150704X.2013.782112.
Malenovský, Z., Homolová, L., Zurita-Milla, R., Lukeš, P., Kaplan, V., Hanuš, J., Gastellu-Etchegorry, J.P., Schaepman, M.E., 2013. Retrieval of spruce leaf chlorophyll content from airborne image data using continuum removal and radiative transfer. Remote Sens. Environ. 131. https://doi.org/10.1016/j.rse.2012.12.015.
McLellan, T.M., Aber, J.D., Martin, M.E., Melillo, J.M., Nadelhoffer, K.J., 1991a. Determination of nitrogen, lignin, and cellulose content of decomposing leaf material by near infrared reflectance spectroscopy. Can. J. For. Res. 21. https://doi.org/10.1139/x91-232.
McLellan, T.M., Martin, M.E., Aber, J.D., Melillo, J.M., Nadelhoffer, K.J., Dewey, B., 1991b. Comparison of wet chemistry and near infrared reflectance measurements of carbon-fraction chemistry and nitrogen concentration of forest foliage. Can. J. For. Res. 21. https://doi.org/10.1139/x91-233.
Moran, J.A., Mitchell, A.K., Goodmanson, G., Stockburger, K.A., 2000. Differentiation among effects of nitrogen fertilization treatments on conifer seedlings by foliar reflectance: a comparison of methods. Tree Physiol. 20. https://doi.org/10.1093/treephys/20.16.1113.
Muhonen, O., Peltola, H., Lauren, A., Ikonen, V.-P., Nevalainen, J., Pikkarainen, L., Kilpeläinen, A., Launiainen, S., Palviainen, M., 2025. Spatial evenness of fertilization and short-term volume growth responses of Scots pine and Norway spruce to fertilization intensity. id 24026. 17 p Silva Fenn. 59 (1). https://doi.org/10.14214/sf.24026.
Nambiar, E.K.S., Fife, D.N., 1987. Growth and nutrient retranslocation in needles of radiata pine in relation to nitrogen supply. Ann. Bot. 60. https://doi.org/10.1093/oxfordjournals.aob.a087431.
Nohrstedt, H.Ö., 2001. Response of coniferous forest ecosystems on mineral soils to nutrient additions: a review of Swedish experiences. Scand. J. Res. https://doi.org/10.1080/02827580152699385.
Rautiainen, M., Stenberg, P., 2005. Application of photon recollision probability in coniferous canopy reflectance simulations. Remote Sens. Environ. 96. https://doi.org/10.1016/j.rse.2005.02.009.
Reich, P.B., Walters, M.B., Ellsworth, D.S., 1991. Leaf age and season influence the relationships between leaf nitrogen, leaf mass per area and photosynthesis in maple and oak trees. Plant Cell Environ. 14. https://doi.org/10.1111/j.1365-3040.1991.tb01499.x.
Reich, P.B., Walters, M.B., Ellsworth, D.S., Uhl, C., 1994. Photosynthesis-nitrogen relations in amazonian tree species - I. Patterns among species and communities. Oecologia 97. https://doi.org/10.1007/BF00317909.
Ribeiro da Luz, B., 2006. Attenuated total reflectance spectroscopy of plant leaves: a tool for ecological and botanical studies. N. Phytol. 172. https://doi.org/10.1111/j.1469-8137.2006.01823.x.
Ribeiro da Luz, B., Crowley, J.K., 2007. Spectral reflectance and emissivity features of broad leaf plants: prospects for remote sensing in the thermal infrared (8.0-14.0 μm). Remote Sens. Environ. 109. https://doi.org/10.1016/j.rse.2007.01.008.
Saarsalmi, A., Mälkönen, E., 2001. Forest fertilization research in Finland: a literature review. Scand. J. Res. https://doi.org/10.1080/02827580152699358.
Savitzky, A., Golay, M.J.E., 1964. Smoothing and differentiation of data by simplified least squares procedures. Anal. Chem. 36. https://doi.org/10.1021/ac60214a047.
Schaepman-Strub, G., Schaepman, M.E., Painter, T.H., Dangel, S., Martonchik, J.V., 2006. Reflectance quantities in optical remote sensing-definitions and case studies. Remote Sens. Environ. 103. https://doi.org/10.1016/j.rse.2006.03.002.
Schlerf, M., Atzberger, C., Hill, J., Buddenbaum, H., Werner, W., Schüler, G., 2010. Retrieval of chlorophyll and nitrogen in Norway spruce (Picea abies L. Karst.) using imaging spectroscopy. Int. J. Appl. Earth Obs. Geoinf. 12. https://doi.org/10.1016/j.jag.2009.08.006.
Sellin, A., 2000. Estimating the needle area from geometric measurements: application of different calculation methods to Norway spruce. Trees Struct. Funct. 14. https://doi.org/10.1007/PL00009765.
Sims, D.A., Gamon, J.A., 2002. Relationships between leaf pigment content and spectral reflectance across a wide range of species, leaf structures and developmental stages. Remote Sens. Environ. 81. https://doi.org/10.1016/S0034-4257(02)00010-X.
Tamm, C.O., 1991. Nitrogen in Terrestrial Ecosystems Questions of Productivity, Vegetational Changes, and Ecosystem Stability. Springer, Berlin.

Ustin, S.L., Gitelson, A.A., Jacquemoud, S., Schaepman, M., Asner, G.P., Gamon, J.A., Zarco-Tejada, P., 2009. Retrieval of foliar information about plant pigment systems from high resolution spectroscopy. Remote Sens. Environ. 113. https://doi.org/10.1016/j.rse.2008.10.019.

Weiss, M., Jacob, F., Duveiller, G., 2020. Remote sensing for agricultural applications: a meta-review. Remote Sens. Environ. 236. https://doi.org/10.1016/j.rse.2019.111402.

Wold, S., Johansson, E., Cocchi, M., 1993. PLS - partial least-squares projections to latent structures. 3D QSAR Drug Design: Theory, Methods and Applications. Kluwer ESCOM Science Publisher, pp. 523–550.

Wright, I.J., Reich, P.B., Westoby, M., Ackerly, D.D., Baruch, Z., Bongers, F., Cavender-Bares, J., Chapin, T., Cornellssen, J.H.C., Diemer, M., Flexas, J., Garnier, E., Groom, P.K., Gulias, J., Hikosaka, K., Lamont, B.B., Lee, T., Lee, W., Lusk, C., Midgley, J.J., Navas, M.L., Niinemets, Ü., Oleksyn, J., Osada, H., Poorter, H., Pool, P., Prior, L., Pyankov, V.I., Roumet, C., Thomas, S.C., Tjoelker, M.G., Veneklaas, E.J., Villar, R., 2004. The worldwide leaf economics spectrum. Nature 428. https://doi.org/10.1038/nature02403.

Yanez-Rausell, L., Malenovsky, Z., Clevers, J.G.P.W., Schaepman, M.E., 2014. Minimizing measurement uncertainties of coniferous needle-leaf optical properties. Part II: experimental setup and error analysis. IEEE J. Sel. Top. Appl. Earth Obs. Remote Sens 7. https://doi.org/10.1109/JSTARS.2013.2292817.

Zarco-Tejada, P.J., González-Dugo, V., Berni, J.A.J., 2012. Fluorescence, temperature and narrow-band indices acquired from a UAV platform for water stress detection using a micro-hyperspectral imager and a thermal camera. Remote Sens. Environ. 117. https://doi.org/10.1016/j.rse.2011.10.007.

Ziechmann, W., 1964. Spectroscopic investigations of lignin, humic substances and peat. Geochim. Cosmochim. Acta 28. https://doi.org/10.1016/0016-7037(64)90006-7.